

Planet Detection Simulations for Several Possible TESS Extended Missions

Luke Bouma^{1,2,3}, Josh Winn^{1,2,3}, Jacobi Kosiarek² and Peter McCullough^{4,5}

¹Department of Physics, 77 Massachusetts Ave., Massachusetts Institute of Technology, Cambridge, MA 02139

²MIT Kavli Institute for Astrophysics and Space Research, 70 Vassar St., Cambridge, MA 02139

³Department of Astrophysical Sciences, Princeton University, 4 Ivy Lane, Princeton, NJ 08540, USA

⁴Space Telescope Science Institute, Baltimore, MD 21218

⁵Department of Physics and Astronomy, Johns Hopkins University, 3400 North Charles Street, Baltimore, MD 21218

The views and opinions expressed in this white paper are those of the authors and do not necessarily reflect the views of the larger *TESS* Science Team. This document has not been endorsed or reviewed by NASA or the *TESS* Science Team.

Executive Summary

The Transiting Exoplanet Survey Satellite (*TESS*) will perform a two-year survey of nearly the entire sky, with the main goal of detecting exoplanets smaller than Neptune around bright, nearby stars. There do not appear to be any fundamental obstacles to continuing science operations for at least several years after the two-year Primary Mission.

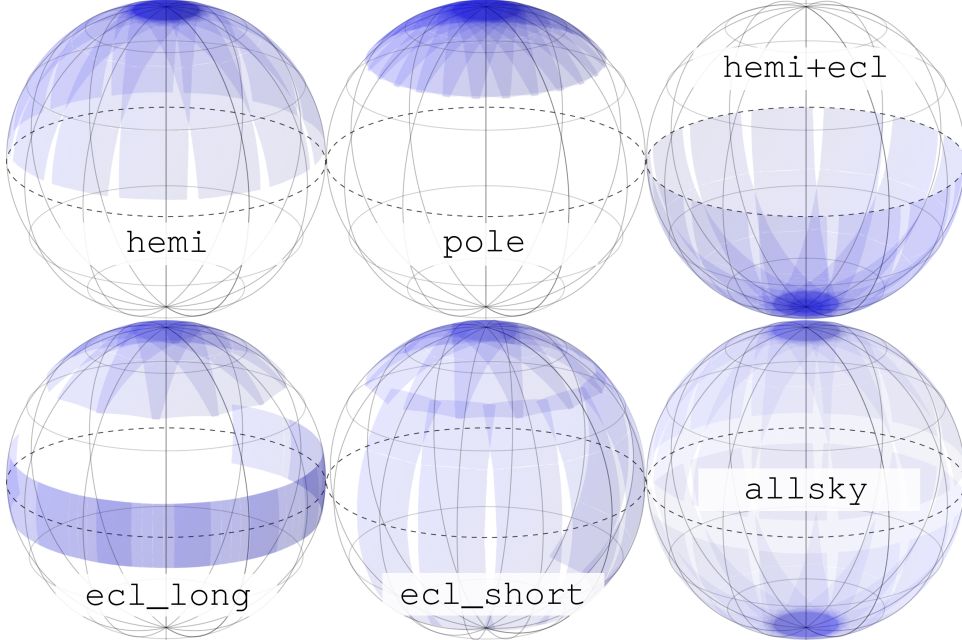
Any decisions regarding use of the *TESS* spacecraft after the Primary Mission should be made with the broadest possible input and assistance from the astronomical community. As has recently been made clear by the NASA *K2* mission, there are many applications of precise time-series photometry of bright objects besides exoplanet detection.

Nevertheless, exoplanet detection is likely to be part of the motivation for a *TESS* Extended Mission. To provide a head start to those who are planning and proposing for such a mission, this white paper presents some simulations of exoplanet detections in a third year of *TESS* operations. Our goal to provide a helpful reference for the exoplanet-related aspects of any Extended Mission, while recognizing that this will be only one part of a larger discussion of the scientific goals of such a mission.

We performed Monte Carlo simulations to try to anticipate the quantities and types of planets that would be detected in several plausible scenarios for a one-year Extended Mission following the two-year Primary Mission. The strategies differ mainly in the schedule of pointings on the sky. For simplicity we did not compare different choices for the cadence of photometric measurements, or for the target selection algorithm, although different choices might prove to be advantageous and should be studied in future work.

We considered six different scenarios for Year 3 of the *TESS* mission, illustrated in Figure 1:

1. `hemi`, which re-observes one of the ecliptic hemispheres in essentially the same manner as in the Primary Mission (i.e., neglecting the zone within 6° of the ecliptic);
2. `pole`, which focuses on one of the two ecliptic poles;
3. `hemi+ecl`, which re-observes an ecliptic hemisphere, but moving all fields 6° closer in latitude to the ecliptic plane. This scenario has a continuous viewing zone with angular diameter 12° rather than 24° ;



4. **ecl_long**, which has a series of pointings with the long axis of the $24^\circ \times 96^\circ$ field-of-view along the ecliptic (in combination with some fields near the ecliptic pole, when the Earth or Moon would prevent effective observations of the ecliptic);
5. **ecl_short**, which has a series of pointings with the short axis of the field-of-view along the ecliptic (again in combination with some fields near the ecliptic pole);
6. **allsky**, which covers nearly the entire sky with ~ 14 -day pointings (as opposed to the 28-day pointings of the Primary Mission), by alternating between northern and southern hemispheres.

We numerically computed the results based on the methodology of Sullivan et al. [2015], after bug fixes and enhancements by Luke Bouma in consultation with Josh Winn. Additional inputs were provided by Jacobi Kosiarek and Peter McCullough.

Some of the most important findings are:

1. The overall quantity of detected planets¹ does not depend strongly on the sky-scanning schedule. Among the six scenarios considered here, the number of newly-detected planets with radii less than $4R_\oplus$ is the same to within about 30%.
2. The number of newly-detected sub-Neptune radius planets ($R_p \lesssim 4R_\oplus$) in Year 3 is approximately the same as the number detected in either Year 1 or Year 2. Thus, we do not expect a sharp fall-off in the planet discovery rate in Year 3. This is because the Primary Mission will leave behind many short-period transiting planets with bright host stars, with a signal-to-noise ratio just below the threshold for detection. These planets can be detected by collecting more data in Year 3.

Figure 1: Six possible pointing strategies for a *TESS* Extended Mission, visualized in ecliptic coordinates. None of these scenarios spend the entire year observing the ecliptic; we concluded that such a plan is inadvisable because of interruptions by the Earth and Moon (see Fig. 9).

¹ We define ‘detected planet’ to mean one with at least two observed transits, and a phase-folded SNR > 7.3 (Eq. 1). All statistics are quoted for $R_p < 4R_\oplus$ planets.

3. Apart from detecting new planets, a potentially important function of an Extended Mission would be to improve our ability to predict the times of future transits and occultations of *TESS*-detected planets. With data from the Primary Mission alone, the uncertainty in planetary orbital periods will inhibit follow-up observations after only a few years, as the transit ephemerides become stale. By re-observing the same sky that was observed in the Primary Mission, `hemi`, `hemi+ecl`, and `allsky` address this issue.
4. Regarding newly detected sub-Neptunes, the `allsky`, `pole`, and `hemi+ecl` strategies offer the greatest number (1350–1400, as compared to the 1250 during each year of the Primary Mission).
5. Regarding planets with orbital periods >20 days, the `allsky` and `pole` strategies discover twice as many such planets as will be discovered in each year of the Primary Mission. However, this assumes that two transits are sufficient for secure detection. If instead we require three transits, then `pole` detects 260 new long-period planets, while the next-best scenarios, `allsky`, `hemi`, and `hemi+ecl`, all detect about 160. (The simulated Primary Mission detects 145; see Figs. 14 and 16).
6. Regarding new planets with very bright host stars ($I_c < 10$), the `allsky`, `hemi+ecl`, and `ecl_short` strategies offer the greatest numbers (≈ 190 , about the same as are found in each year of the Primary Mission; see Table 2).
7. Regarding planets with near-terrestrial insolation ($0.2 < S/S_\oplus < 2$), all the strategies considered here offer similar numbers (about 120, as compared to 105 in each year of the simulated Primary Mission).

The rest of this report is organized as follows. Sec. 1 discusses how we selected and compared different pointing strategies, as well as how we modeled *TESS*'s observations. Sec. 1.3 describes some figures of merit for comparing Extended Mission scenarios, including a discussion of some scenarios we chose not to study. Sec. 1.7 lists the most important assumptions we made for the simulations. Sec. 2 compares the characteristics of newly-detected planets, for the 6 different scenarios under consideration. Sec. 3.1 discusses some considerations and implications for future years of the Extended Mission, beyond the one-year scenarios that were simulated in detail. Sec. 3.2 discusses the critical issue of the uncertainty in transit ephemerides. Sec. 3.3 discusses the reliability and limitations of our methodology. Sec. 4 concludes and recommends avenues for further study.

The catalogs of simulated detected planets (for both the Primary and Extended Missions) are available online². This web site also contains a less formal document with some ideas and questions regarding the broader applications of a *TESS* Extended Mission. We welcome any other ideas, comments, or corrections; please send them to: `luke@astro.princeton.edu`.

² [url_goes_here.com](#)

Contents

1 Approach	5
1.1 Constraints on <i>TESS</i> 's Observing	5
1.2 Proposed Pointing Strategies	6
1.3 Metrics to Compare Pointing Strategies	8
1.4 Description of Planet Detection Model	11
1.5 Selecting Target Stars (and Modelling Full Frame Images)	13
1.6 Earth and Moon Crossings	17
1.7 Summary of Key Assumptions and Attributes of Planet Detection Simulations	23
2 Planet Detection Statistics	25
2.1 Planet Yield from the Primary Mission	26
2.2 Planet Yield from Example Extended Mission: hemi . . .	27
2.3 Comparing Planet Yields from all Extended Missions . .	30
2.4 On the Brightness of Stars with Detected Planets	39
3 Discussion	40
3.1 Planning Year 3 with Years 4–N in mind	40
3.2 The Ephemeris Problem	41
3.3 Risks and Caveats	45
4 Concluding remarks and recommendations	48
4.1 Recommendations	48
Appendices	52
Appendix A Models Relevant to Earth and Moon Crossings	52
Appendix B Lens Hood Model: Additional Count Rate from Arbitrary Source	54
Appendix C Changes from Sullivan et al. [2015]	57
References	58

1 Approach

1.1 Constraints on TESS's Observing

When considering possible schedules for telescope pointings, the main constraint is that the cameras must be directed approximately opposite the Sun. Specifically, the center of the combined fields-of-view is ideally pointed within 15° in ecliptic longitude of the anti-solar direction, and no more than 30° away. This enables the solar panels to collect sufficient sunlight to power the spacecraft. Fig. 2 illustrates the geometry. The solar panels are free to rotate about the Y-axis.

It is also important for the sunshade and spacecraft to block sunlight. This constraint makes it difficult to remain pointed at a given field for more than two spacecraft orbits (≈ 42 days). This is why *TESS* advances the fields of view by $\approx 28^\circ$ east in ecliptic longitude every lunar month, during the Primary Mission. Another important consideration is whether the Earth or Moon passes through *TESS*'s camera fields during a proposed pointing (see Sec. 1.6), because these crossings are detrimental to high photometric precision.

In addition, the spacecraft has finite fuel reserves for necessary maneuvers. These are expected to last at least 10 years [G. Ricker, priv. comm.]. Since the time horizon for this study is only 3 years, we do not consider the fuel reserves to be a constraint on the scenarios we investigate.

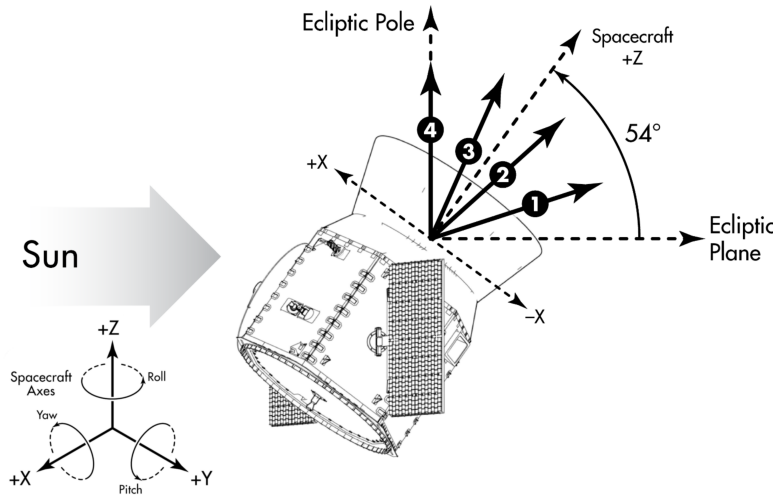


Figure 2: The spacecraft must point so that incident sunlight is collected by the solar panels, and not the cameras. *TESS*'s solar panels pitch about the +Y axis. (Adapted from Orbital ATK design document)

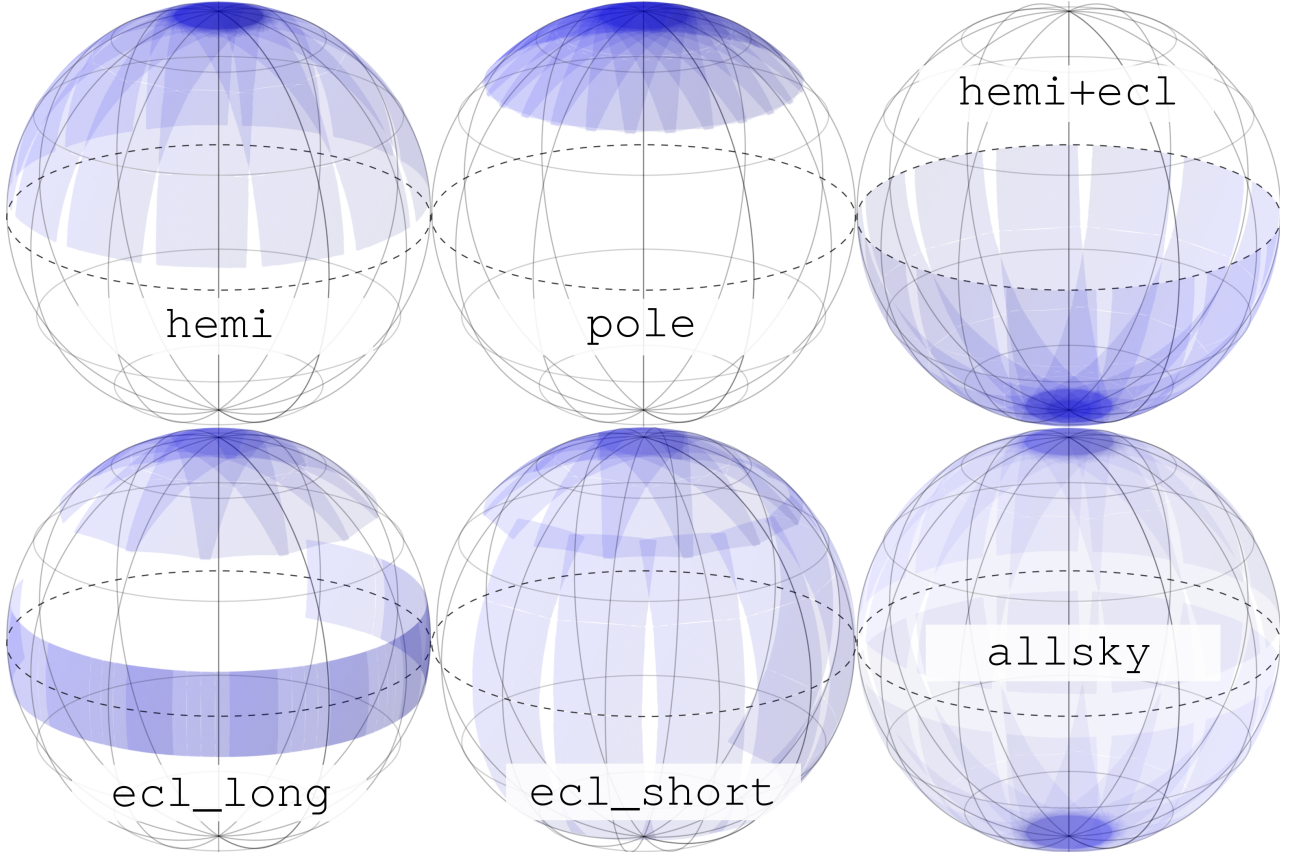


Figure 3: Proposed pointing strategies for a *TESS* Extended Mission, visualized in ecliptic coordinates. *hemi*, *pole*, *hemi+ecl*, *ecl_long*, *ecl_short*, and *allsky*. Note for *ecl_long* and *ecl_short* that Earth and moon crossings likely make an entire year looking at the ecliptic impractical (see Fig. 9).

1.2 Proposed Pointing Strategies

For simplicity we chose to study one-year plans for an Extended Mission, i.e., plans for Year 3 of the *TESS* mission. (Later in this report we remark on some possible implications of our study for additional years of an Extended Mission.) Given the constraints outlined in Sec. 1.1, we selected the following scenarios for detailed study:

Scenario 1. *hemi*: Repeat observations of one of the two ecliptic hemispheres in a manner similar to the Primary Mission. For concreteness we arbitrarily chose the northern ecliptic hemisphere for the third year. In this scenario we could take the opportunity to shift the longitudes of all sectors by an amount that would enable *TESS* to cover the gaps that were left during the Primary Mission (the “slits” in the sky coverage between ecliptic latitudes of 6–30°). However for simplicity, we opted to observe the same longitudes as in the Primary Mission. *Motivation:* similar to the Primary Mission. Long time baseline at the North Ecliptic Pole, and broad sky coverage. Also remeasures transit times (and substantially

improves ephemerides) of previously detected *TESS* planets over most of the entire hemisphere.

Scenario 2. pole: Focus on one of the ecliptic poles, arbitrarily chosen to be the north ecliptic pole for concreteness. *TESS*'s sunshade and lens hoods must still suppress incoming sunlight in this scenario. A potential problem is sunlight might reflect off the interior of the sunshade and into a lens hood. Since this problem could be addressed by rotating the spacecraft to point slightly anti-Sun (putting the cameras in the shadow of the sunshade), we neglect any effects of extra scattered sunlight³. *Motivation:* maximizes the average duration of observations per star; intuitively expected to provide greatest sensitivity to long-period planets.

Scenario 3. hemi+ecl: Repeat observations of one of the two ecliptic hemispheres, but in this case shifting all fields 6° toward the ecliptic, such that the combined fields-of-view reach all the way from the ecliptic to 6° behind the ecliptic pole. We chose to simulate the southern ecliptic hemisphere because the northern version of this plan would suffer more from Earth and Moon interference (cf. Table 1 in Sec. 1.6). *Motivation:* trades the long continuous viewing zone near the pole for greater sky coverage, and in particular, coverage of the ecliptic zone which was missed in the Primary Mission. Extensible to Year 4. Freshens ephemerides.

Scenario 4. ecl_long: Survey the ecliptic with 7 sectors (14 orbits) in which the long axis of the fields-of-view are oriented along the ecliptic. For the other 6 sectors, during the interval when ecliptic observations would be interrupted by Earth and Moon crossings, we focus on one of the ecliptic poles. *Motivation:* covers the ecliptic, which will not be observed during the Primary Mission. Offers opportunities for follow-up of K2 discoveries. Minimizes Earth-moon interference.

Scenario 5. ecl_short: Survey the ecliptic and also cover a large fraction of the rest of the ecliptic hemisphere. For 7 sectors we observe the ecliptic but with the *short* axis oriented along the ecliptic, and the long axis reaching up to higher latitudes. The remaining 6 sectors are focused on the ecliptic pole, as in *ecl_long*. *Motivation:* similar to *ecl_long*, but with more overlap between this year and the Primary Mission to allow for improved transit ephemerides and better ability to follow-up on previous discoveries. Also covers more sky than *ecl_long*, which could improve the quantity of planet detections from full frame images.

Scenario 6. allsky: Cover both northern and southern ecliptic hemispheres in a single year, by alternating between the hemispheres

³ Whether this minor adjustment would even be necessary depends on the combined performance of the sunshade and each camera's lens hood. These will be verified by measurements during commissioning.

every 13.7 days. *Motivation:* rapid coverage of the entire sky, allows follow-up of almost all previously detected *TESS* objects and refined ephemerides.

Although these 6 scenarios seemed like reasonable choices for further study and direct comparison, there are many other possibilities that may be of interest that were not studied in detail, in order to keep the scope of this report manageable. Among these other possibilities that were considered but not studied are

- The `pole` strategy applied to the south ecliptic pole rather than the north (we do not expect major differences).
- The `hemi` strategy applied to the southern ecliptic hemisphere rather than the northern (we do not expect major differences).
- The `hemi` strategy, but rotated about the ecliptic polar axis by 12° in longitude.
- The Northern inversion of `hemi+ecl`, which is more strongly affected by Earth and Moon crossings (Sec. 1.6) and is less able to improve knowledge of mid-transit times (Fig. 23).
- A version of `hemi` in which all fields are 12° closer to the ecliptic, rather than 6° as in `hemi+ecl`.
- A full year spent observing the ecliptic. Such a plan would suffer from Earth and Moon crossings for a substantial fraction of the year. We show the outage as a function of time in Fig. 9. Solar system objects (planets, asteroids) could also be an annoyance, although we did not model their effects.
- Alternate between northern and southern ecliptic poles every 13.7 days. This would be similar to `allsky` but would focus on the poles rather than the entire sky. It would sacrifice sky coverage (and ability to refresh ephemerides over the whole sky) in return for a longer mean observation duration per star.
- Hybrid strategies that change from month to month. For instance, in the `hemi` scenario, during a month when the Earth or Moon crosses through the field of a camera pointed close to the ecliptic, we could tilt all the cameras away from the ecliptic as in the `pole` scenario.

1.3 Metrics to Compare Pointing Strategies

We assess Extended Missions based on the risks and opportunities they present, as well as their performance on selected technical

and science-based criteria. These criteria are organized following an approach originally outlined by Kepner and Tregoe [1965]. Summarizing them in list form:

Technical musts: Point cameras anti-sun. Allow the solar panels to collect sunlight.

Technical wants: Keep the duration of each sector < 28 days. Minimize Earth or Moon crossings. Minimize zodiacal background light. Minimize scattered sunlight.

Metrics in exoplanet science:

- number of newly detected planets
 - from stars observed with 2-minute time sampling from among $\approx 200,000$ subrasters, known colloquially as "postage stamps" (PS),
 - from stars observed with 30-minute time sampling in the full-frame images (FFIs);
- number of new long-period planets
 - by detecting additional transits of planets for which only one transit was observed in the Primary Mission,
 - by detecting transits of long-period planets that were not detected in the Primary Mission;
- number of new habitable-zone planets;
- number of new planets with "characterizable" atmospheres;
- number of newly detected planets with bright host stars;
- number of planet-hosting stars detected in the Primary Mission for which the Extended Mission reveals an additional transiting planet;
- ability to improve transit ephemerides for previously detected transiting planets;
- ability to observe more transits over a longer baseline to enable searches for transit-timing variations.

These metrics were chosen for their apparent importance as well as our ability to quantify them with simulations. Of course there are other considerations that may be very important but are more difficult to quantify:

- Different ways to choose the stars that are observed with finer time sampling. It will likely be advantageous to use the results of the Primary Mission to choose stars for which photometric variability is known to be detectable and interesting. Examples include planet

hosts, candidate planet hosts, circumbinary & circumprimary planets, white dwarfs, open clusters, eclipsing binaries and higher-order systems, pulsating stars (Cepheids, RR Lyrae, δ Scuti, slowly pulsating B stars), eruptive stars, cataclysmic variables, and stars of special interest for asteroseismology.

- Prospects for solar-system science, such as observations of main belt asteroids and the brightest near-Earth asteroids.
- Prospects for extragalactic astronomy and high energy astrophysics; for instance, gathering light curves of variable active galactic nuclei, or imaging extended low surface brightness features of galaxies.

Regarding opportunities and risks, the following need to be considered:

Opportunities:

- Optimizing science beyond the 3-year horizon. For example, suppose it were known in advance that *TESS* would likely continue operations for 5-10 years: how would this knowledge affect the decision on what to do in the year following the Primary Mission?
- Ability to promote targets that were detected in FFIs to PSs in the Extended Mission.
- Alter the number of PSs, the time sampling of the PS, and the time sampling of the FFIs, under the constraint of fixed data volume. An extreme case is eliminating the PSs and returning only FFIs.
- *TESS as follow-up mission:* ability to observe *CoRoT* objects; ability to observe the *Kepler* field; ability to observe *K2* fields (follow-up *K2* few-transit objects); ability to observe targets previously monitored by ground-based surveys.
- *Prospects for follow-up with other resources:* potential for *JWST* follow-up, potential for *CHEOPS* follow-up, ability to obtain *TESS* photometry contemporaneously with ground-based observations, ability to follow up with resources in both hemispheres.
- Impact on Guest Investigator program.

Risks: Risk of spacecraft damage. Risk of not meeting threshold science (however it is defined for the Extended Mission). Risk of poorer photometric precision than desired, e.g., from confusion in crowded fields. Would partial instrument failure in Primary Mission make this scenario infeasible? Would reduced precision (from

aged CCDs, worse pointing accuracy, or other mechanical sources) invalidate this scenario? Risk of planet detection simulation over- or under-estimating planet yield.

1.4 Description of Planet Detection Model

Sullivan et al. [2015] (hereafter, S+15) developed a simulation of *TESS*'s planet and false positive detections based on the spacecraft and payload design specified by Ricker et al. [2014]. We adapt this simulation for Extended Mission planning. With our additions, we can change where *TESS* looks in additional years of observing while holding fixed all other mission-defining parameters. Our approach is to run our planet detection simulation for each plausible pointing strategy, and to compare the relative yields of detected planets. This lets us compare Extended Mission scenarios with one another and with the Primary Mission.

Background on synthetic catalogs: *TESS* is sensitive to sub-Neptune sized transiting planets orbiting M dwarfs out to ~ 200 pc and G dwarfs out to ~ 1 kpc (S+15, Sec. 2.3). It is sensitive to giant planets and eclipsing binaries across a significant fraction of the galactic disk. With this sensitivity in mind, the stellar catalog we ‘observe’ in our planet detection simulation is drawn from the output of TRILEGAL, a population synthesis code for the Milky Way [Girardi et al., 2005]. S+15 made some modifications to the catalog, notably in the M dwarf radius-luminosity relation, to better approximate interferometric stellar radii measurements. We retain these modifications; the modified TRILEGAL stellar catalog shows acceptable agreement with observations⁴, specifically the Hipparcos sample [Perryman et al., 1997, van Leeuwen, 2007] and the 10pc RECONS sample [Henry et al., 2006].

With a stellar catalog defined, we populate the stars in the catalog with planets based on occurrence rates derived from the *Kepler* sample. We use rates Fressin et al. [2013] found for planets orbiting stars with $T_{\text{eff}} > 4000$ K and those that Dressing and Charbonneau [2015] found for the remaining M and late K dwarfs.

Detection process: We then simulate transits of these planets. Assuming the transit depth and number of transits are known, we use a model of *TESS*'s point spread function (PSF) to determine optimal photometric aperture sizes for each postage stamp star (*i.e.*, we compute the noise for all plausible aperture sizes, and find the number of pixels that minimizes this noise). With the aperture sizes and noise corresponding to a given integration time known, we compute a signal to noise ratio for each transiting object. Our model for planet

⁴ Looking closely at the radius-luminosity relations, we do see non-physical interpolation artifacts. These outliers are visible in Figs. 5 and 6 below, but are a small enough subset of the population that we ignore them for this work.

detectability is a simple step function in SNR: if we have two or more transits and $\text{SNR} > 7.3$, the planet is ‘detected’, otherwise it is not detected⁵. Cast as an equation,

$$\text{Prob(detection)} = \begin{cases} 1 & \text{if } \text{SNR}_{\text{phase-folded}} > 7.3 \text{ and } N_{\text{tra}} \geq 2 \\ 0 & \text{otherwise,} \end{cases} \quad (1)$$

for N_{tra} the number of observed transits and $\text{SNR}_{\text{phase-folded}}$ the phase-folded signal to noise ratio, defined in Eq. 2 below. Our model for *TESS*’s photometric precision is described by S+15 and also shown in Fig. 7.

Assumptions of SNR calculation: A realistic simulation of the signal detection process would begin with a realistic noise model for each 2-second CCD readout, taking into account both instrumental and astrophysical variations. These 2-second data would be stacked into 2-minute averages for the PSs and 30-minute averages for the FFIs. The time series would then be prepared and searched for transit signals using the same code that is used on real data. Our calculation is much simpler. We calculate the total SNR based on all the data points collected during transits, with a simple threshold value of 7.3 for detection. We implicitly assume that the correct period can be identified and that the noise follows the simple model of S+15, which includes instrumental noise and an empirically-determined level of stellar variability.

We also assume the transit signal to be constant in amplitude, although it may be reduced in amplitude (“diluted”) below $(R_p/R_\star)^2$ due to the constant light from other stars that fall within the same photometric aperture. Our approach is then to simply tally the number of *TESS* fields a given host star falls within, which corresponds to a known total observing baseline. Knowing a planet’s orbital period, and assuming the planet is randomly phased in a circular orbit when *TESS* begins observing, we then count the number of transits *TESS* observes for the planet over the total baseline.

Using a model PSF, we determine ideal aperture sizes and obtain an estimated noise per transit. Summarizing the relevant terms in an equation,

$$\begin{aligned} \text{SNR}_{\text{phase-folded}} &\approx \sqrt{N_{\text{tra}}} \times \text{SNR}_{\text{per-transit}} \\ &= \sqrt{N_{\text{tra}}} \times \frac{\delta \cdot D}{\left(\frac{\sigma_{\text{lhr}}^2}{T_{\text{dur}}} + \sigma_v^2 \right)^{1/2}}, \end{aligned} \quad (2)$$

for δ the undiluted transit depth; D the dilution factor computed from background and binary contamination (Eq. 4); σ_{lhr} the summed

⁵ The value of this threshold is chosen to ensure that no more than one statistical false positive is present in a pipeline search of 2×10^5 target stars. When observing a greater number of stars, for instance in the full frame images, a higher threshold value should be imposed to maintain the same condition. We discuss this further in Sec. 3.3.

noise contribution from CCD read noise, photon-counting noise from the star, a systematic $60 \text{ ppm} \cdot \text{hr}^{1/2}$ noise floor, and zodiacal noise; T_{dur} the transit duration in hours, and σ_v the intrinsic stellar variability (cf. S+15 Sec 3.5). Note that our only noise contribution which is not white comes from stellar variability, which following S+15 we assume to be independent over transits and also independent of the duration of a given transit. Finally, we multiply the SNR per transit by the square root of the number of transits observed.

We have changed some aspects of this simulation since the work by S+15 was published. These changes are described in Sec. C.

1.5 Selecting Target Stars (and Modelling Full Frame Images)

For the Primary Mission, *TESS*'s short cadence (2 min) targets will be drawn from a subset of the *TESS* Input Catalog. The exact manner in which these targets will be chosen has not yet been determined.

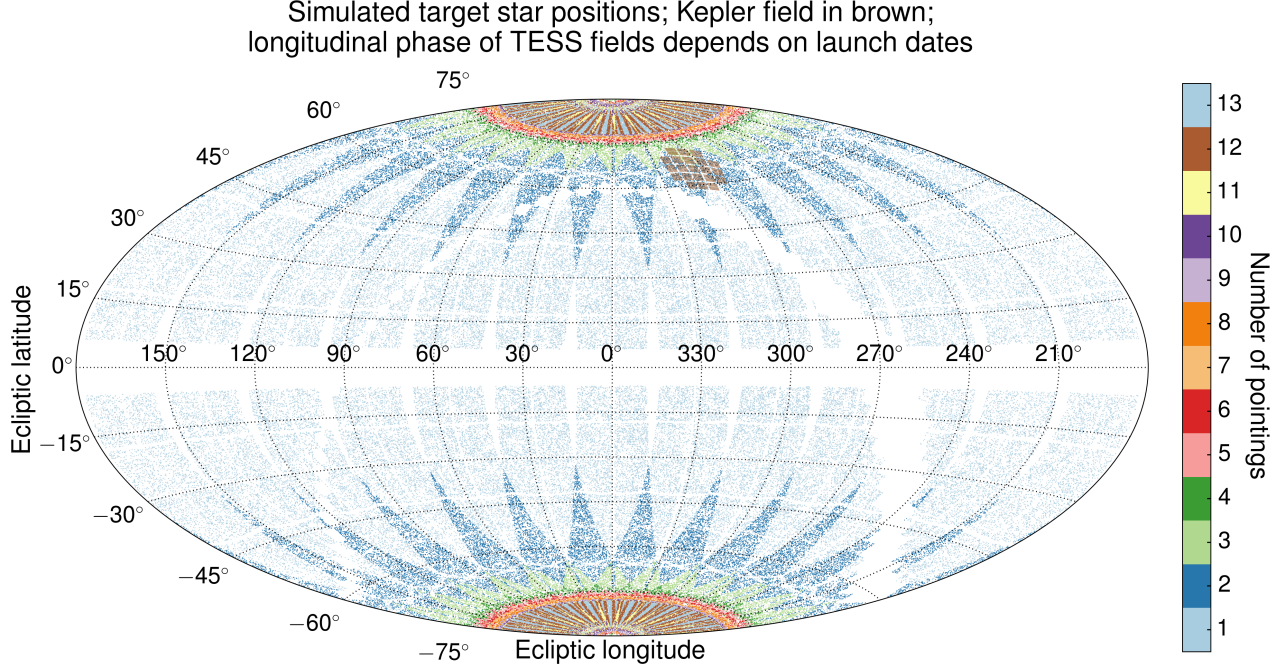
We know that for *TESS* to detect small transiting planets it should observe stars that are small and bright. For this work, we define a simple statistic, **Merit**, proportional to the SNR we should expect from a given planet orbiting the star:

$$\text{Merit} \equiv \frac{1/R_*^2}{\sigma_{\text{1-hr}}(I_c)/\sqrt{N_{\text{obs}}}}, \quad (3)$$

where R_* is the radius of the star in question, $\sigma_{\text{1-hr}}$ is the relative precision in flux measurements over one hour of integration time, taken from an empirical fit to Fig 7, I_c is the Cousins band I magnitude *TESS* observes for the star (or more precisely, the star system) and N_{obs} is the number of observations the star receives over the course of the mission. For multiple star systems, R_* is taken to be the radius of the planet-hosting star, and the I_c magnitude is computed from the combined flux of all the stars.

We evaluate **Merit** for all the star systems in our modified TRI-LEGAL catalog, and then choose the highest-Merit 2×10^5 as target stars to be observed at 2 minute cadence. Target stars selected in this manner are shown in Fig. 4. This statistic is simpler than the procedure outlined in Section 6.7 of S+15 and it produces a nearly identical population of target stars (shown in Fig 5). Our approach for full frame image simulation is different from that of S+15, and we describe it below.

We generalize our **Merit** statistic to Extended Missions as follows: over an entire mission, the total number of observations a star receives is the sum of its observations in the Primary and Extended Missions: $N_{\text{obs}} = N_{\text{primary}} + N_{\text{extended}}$. If $N_{\text{extended}} = 0$ for a given star, then do not select that star as a target star in the Extended Mission. Else, compute its **Merit** (Eq. 3) substituting



$N_{\text{obs}} = N_{\text{primary}} + N_{\text{extended}}$. In this manner stars that are observed more during the Primary Mission are more likely to be selected during the Extended Mission.

Alternative prioritization approaches: It is worth emphasizing that our scheme for selecting target stars for an Extended Mission does not make use of any information on whether candidate transit events were detected during the Primary Mission. If a star were observed at short cadence for an entire year, and no candidate events were found, it might be sensible to disregard that star in the Extended Mission in favor of stars that have never been observed at short cadence – particularly those with candidate events that were detected in the Primary Mission full-frame images. These and related concerns are discussed further in the accompanying document??.

More abstractly, the procedure of simply applying Eq. 3 attempts to select a stellar sample that will yield the most small transiting planets around the brightest stars. An alternative approach would be to select stars that will give the most *relative benefit* in 2 minute postage stamps over 30 minute cadence observations since all stars will be present in the 30 minute images. This ‘relative benefit’ could be based on improvement in transit detectability, or perhaps improved capacity to resolve the partial transit phases.

Figure 4: Selected target stars in the Primary Mission. Their surface density increases as $\sqrt{N_{\text{obs}}}$ towards the poles because of the weight used in Eq. 3. Gaps in the focal plane array between each of a given camera’s four CCDs leads to the slight deviations from continuous observing at the ecliptic pole.

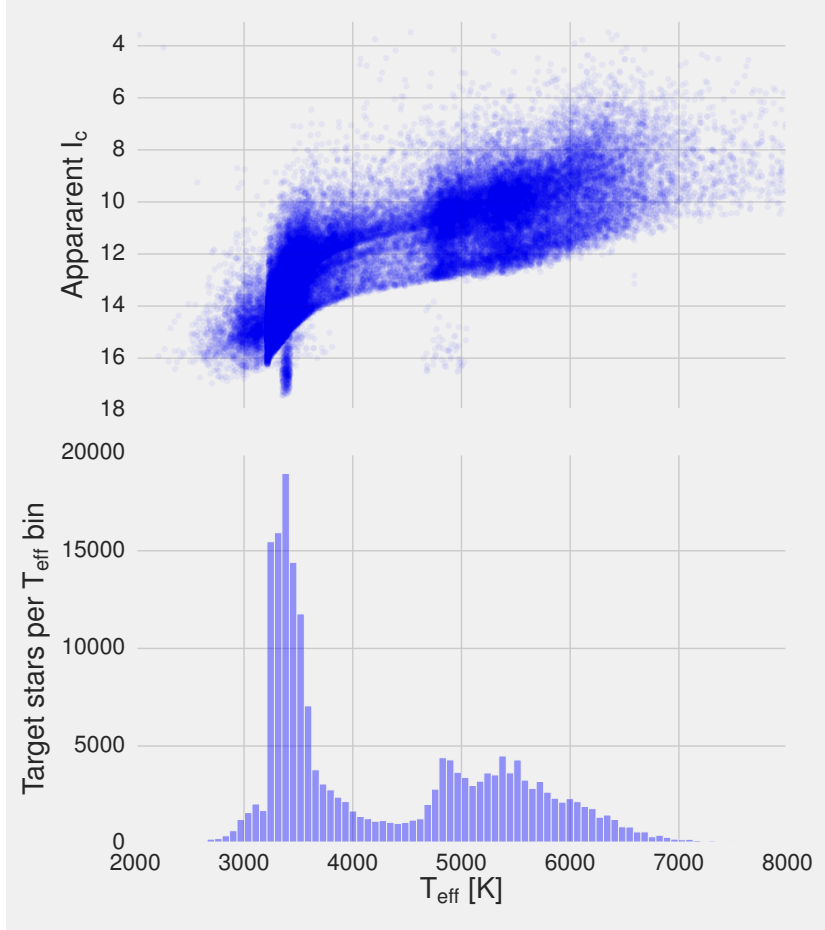


Figure 5: Target star Cousins I magnitude against effective temperature (replicates Figure 17 of S+15). Target stars are selected as the best 2×10^5 stars according to $\text{Merit} \equiv \sqrt{N_{\text{obs}}(1/R_*^2)/\sigma_{1\text{-hr}}(I_c)}$. The top subplot shows 1 in 10 stars. This simple model could inform the target selection to be performed on the TESS Input Catalog. The lower histogram is bimodal, selecting heavily for M dwarfs, and selecting more F and G dwarfs than K dwarfs. This shape arises from the combined $1/R_*^2$ and $1/\sigma_{1\text{-hr}}(I_c)$ weights: the fact that the minimum falls between FG and M stars is because there are many more FG stars than K stars in our catalog, and because M stars offer the largest signals. Note also the dip in the TRILEGAL (& observed) V -band luminosity functions for K stars (see S+15 Figure 5).

The outliers visible in the upper scatter plot represent nonphysical "stars", possibly artifacts of the Padova-to-Dartmouth conversion performed by S+15. These comprise fewer than 1% of the target stars, and are ignored in what follows.

For purposes of transit detection, the difference between 2 and 30 minute cadence matters most when transits have short durations – in other words for small stars, and for close-in planets. Switching to this alternative approach would consequently bias us even more strongly toward selecting M dwarfs. We already select almost every M dwarf with $I_c < 14$. The limiting I_c magnitude for detecting $R_p > 4R_\oplus$ planets with *TESS* is ~ 16 , which is where we see the dimmest stars in Fig. 5.

Additionally, the procedure of applying Eq. 3 and assuming that it will maximize the number of small planets that *TESS* will detect about bright stars ignores the dependence of planet occurrence rates on stellar properties, or on the properties of planets already known to exist around those stars. If the goal is literally to maximize the number of planet detections (a goal which we do not advocate) then *TESS*'s target selection might take these dependences into account. For example the planet occurrence rates measured with *Kepler* data

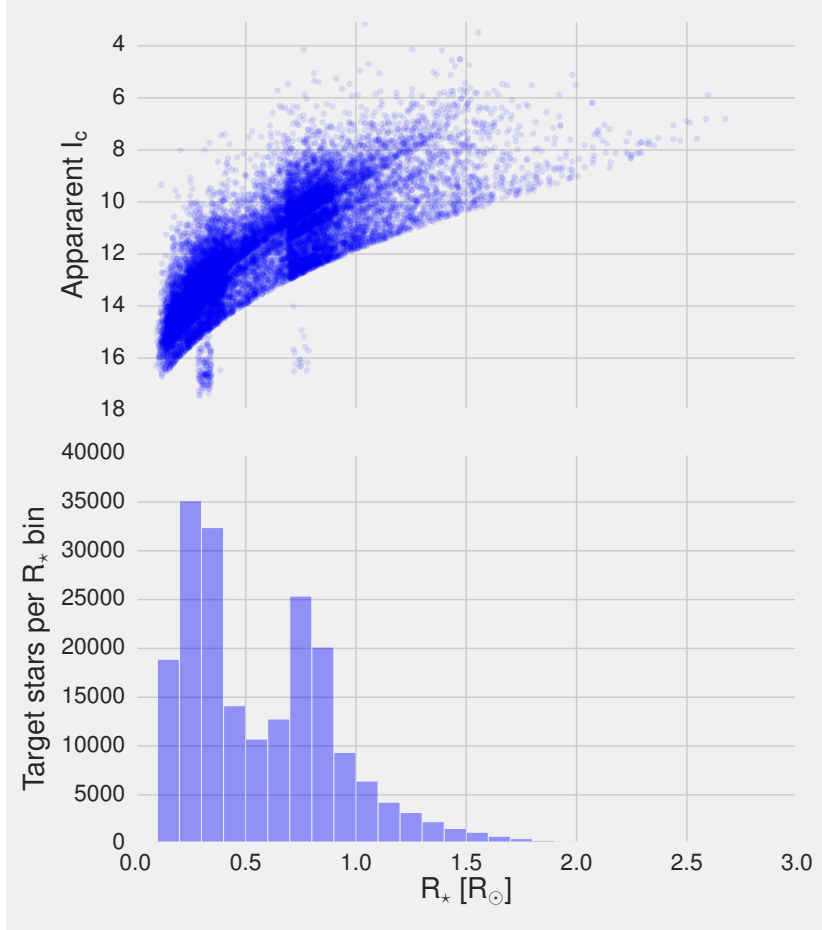


Figure 6: Same as Fig. 5, but as a function of stellar radius. $1/R_*^2$ selection weight visible, along with the same outliers.

could be used to upweight those types of stars most likely to have planets. Likewise Kipping and Lam [2016] note that the probability for a star with short-period transiting planets to have additional transiting planets is dependent upon the radii and periods of the short-period planets. They navigate the optimization problem using artificial neural networks (ANNs) trained to select for features that improve the probability of detecting transiting outer companions. *TESS* might benefit from a similar approach in target selection.

Alternative prioritization approaches in Extended Missions: Our Merit statistic also neglects the possibility of an Extended Mission which only observes stars with known planets or planet candidates (*TESS*'s objects of interest, or those from other transit and RV surveys) at short cadence. This approach would free up a considerable portion of *TESS*'s data mass for full frame images at e.g., 15 minutes rather than the current nominal 30 minutes.

Approach to full-frame images: We want to simulate the full frame image detections in a computationally tractable manner. While S+15 evaluated the phase-folded SNR for every potentially transiting object about each of the $\sim 1.6 \times 10^8$ stars in our synthetic catalog, we consider only the stars for which *TESS* could plausibly detect a sub-Neptune planet during a 3-year mission. Most stars that *TESS* sees are too dim or too large to detect $R_p < 4R_{\oplus}$ planets – while we expect many giant planet detections towards the galactic plane (S+15 Fig 19), small-planet detections are more nearly isotropic, since practically all occur for stars at < 1 kpc. While thousands of transiting giant planets will be revealed by *TESS*, we assume here that the prospects for detecting smaller planets are more likely to help discriminate between different scenarios for the Extended Mission.

In this vein, we only simulate full frame image detections for the 3.8×10^6 highest Merit stars following the 2×10^5 highest Merit stars that are selected for 2-minute observations. This number (3.8×10^6) was initially estimated based on the number of searchable stars about which we expect *TESS* to be able to detect sub-Neptune radius planets [Winn, 2013b]. Our model for the detection process for the FFI data is identical to that of the PS data, except that the effects of time-smearing on the apparent transit duration and depth are taken into account (which is important for durations $\lesssim 1$ hour).

To check that the 4×10^6 highest Merit stars includes all stars about which *TESS* might detect sub-Neptune radius planets, we repeated this process for the Primary Mission using 5.8×10^6 , 9.8×10^6 and 19.8×10^6 ‘full frame image’ stars, and confirmed that there was no significant difference in the planet yields at $R_p \leq 4R_{\oplus}$ between any of the cases. With an increased number of FFI stars, the number of detected giant planets also increased, particularly near the galactic disk. Meanwhile the number of sub-Neptune planets remained fixed. This convinced us that 4×10^6 is a sufficient number of target stars to compute detection statistics for sub-Neptune planets.

1.6 Earth and Moon Crossings

When the Earth or Moon passes through *TESS*’s camera fields, the CCD pixels are flooded to their full well capacity ($\sim 2 \times 10^5$ photo-electrons). Precision differential photometry becomes impossible in any pixels that are directly hit during these crossings. Even when the Earth or Moon is not directly in the camera’s field of view, light may scatter off the interior of spacecraft’s lens hood and act as a source of contaminating flux across many of the cameras. The Poisson noise in the number of photons arriving from the Earth or the Moon in such a scenario degrades *TESS*’s photometric performance, although a

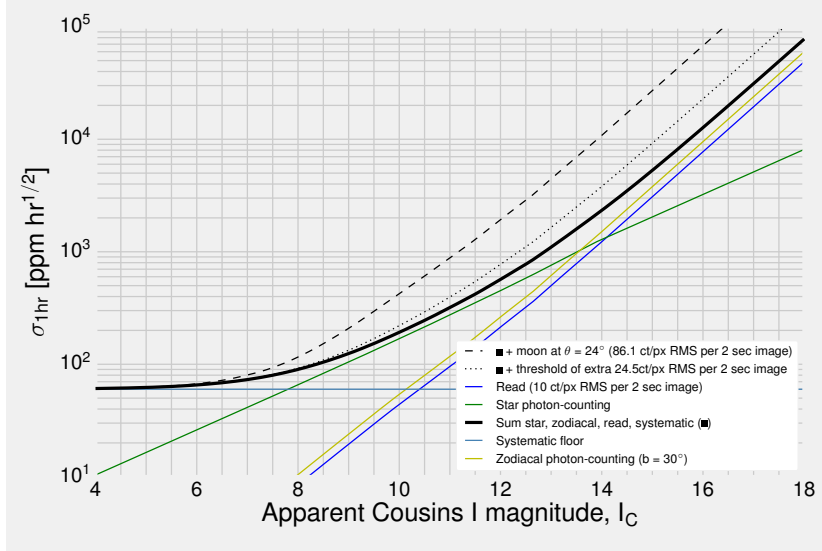


Figure 7: Relative precision in measured flux over a one hour integration time. The noise sources described by Sullivan et al. [2015] are solid thin lines. Additional scatter from contaminating background stars is not shown. The dashed-dot line corresponds to the predicted noise budget with an additional background flux from the Moon at 24° from a camera’s boresight. The dotted line corresponds to the predicted noise budget including an additional threshold flux, $F_{\text{thresh}} \equiv 300 \text{ ct}/\text{px}/\text{s}$, that we use to flag Moon and Earth contamination in *TESS*’s field of view (see text). Zodiacal background is plotted for an ecliptic latitude of 30° using Eq. 21 of Sullivan et al. [2015]. The appended Figs. 27–29 show this plot with scattered sunlight, moonlight, and Earthlight at arbitrary angles.

detailed model for the scattered light is not yet available.

We first illustrate with an example. When the Moon is 24° from a camera boresight the lens hood is expected to suppress $1/100^{\text{th}}$ of a mean $3 \times 10^6 \text{ ct}/\text{px}$ (per 2 second image) from incoming moonlight⁶. Thus a mean flux of $3 \times 10^4 \text{ ct}/\text{px}$ reaches the cameras per image. Assuming the arrival of these photons is Poissonian, the additional RMS is then $173 \text{ ct}/\text{px}$ per 2 second image. Including this additional variance in the quadrature sum of variances of all noise sources, Fig. 7 shows that this background is the dominant noise source for stars with $I_c \gtrsim 8$ – nearly all target stars. While the effect’s magnitude is highly dependent on the angle between a camera’s boresight and the Moon or Earth, the general picture is that for field angles $\theta \lesssim 25^\circ$, the impact can be severe.

Separately from our planet detection simulation, we study these crossings in a dynamical simulation based on JPL NAIF’s standard SPICE toolkit. Given a nominal launch date (we assume Dec 20, 2017), this code determines *TESS*’s orbital phasing throughout its entire mission. At every time step of the three-body orbit, we calculate the distance between *TESS* and the other two bodies of interest, and the separation angles among each of the four cameras and each of the two bodies (eight angles in total). The spacecraft’s inclination oscillates in the simulation as it will in reality.

Taking the Earth and Moon’s integrated disk brightnesses as fixed values⁷ we use a model for scattered light suppression from the *TESS* lens hoods (Fig. 25) to compute the mean photon flux from each of these bodies onto each of the cameras throughout the orbit.

⁶ Our model for suppression as a function of angle is appended in Fig. 25. We implicitly assume 100% quantum efficiency, so photons, electrons, and counts are interchangeable; $1 \text{ ph} = 1 \text{ e}^{-1} = 1 \text{ ct}$.

⁷ The full moon’s apparent magnitude is $I_D \approx -13.5$. Scaling from photon fluxes tabulated in Winn [2013a], this gives $2.5 \times 10^{13} \text{ ct}/\text{s}$. Averaging over the number of pixels in the focal plane array, this gives a mean additional flux per image of $3 \times 10^6 \text{ ct}/\text{px}$. The Earth will contribute a mean flux ~ 80 times greater. This substantiates the claim that the Earth and Moon flood the cameras to their full well capacity. The effect on observing precision is appended in Fig. 26.

	Camera 1	Camera 2	Camera 3	Camera 4
Year 3 selected				
pole	0	0	0	0
hemi	2	1	0	0
hemi+ecl	2	0	0	0
ecl_long	1	1	1	1
ecl_short	0	1	1	0
allsky	1	1	0	0
Year 3 omitted				
pole (south)	0	0	0	0
hemi (south)	1	0	0	0
hemi+ecl (north)	4	3	0	0
ecl_long (1yr)	4	4	4	4
ecl_short (1yr)	1	3	4	2
allsky (poles)	0	0	0	0
Primary Mission				
hemi (south year 1)	2	1	0	0
hemi (north year 2)	4	2	0	0

Table 1: Number of sectors (of 13 per year) ‘dropped’ due to the Earth and Moon crossings in both selected and omitted Extended Missions, with those of the Primary Mission for reference. The method of ‘dropping’ fields (which neglects the temporal nature of the crossings, discussed in the text) gives an approximate sense of the cumulative impact of Earth and Moon crossings. Scenarios with (south) or (north) appended refer to their counterparts in that hemisphere. `ecl_long` (1yr) corresponds to a full year with the long axis of *TESS*’s field of view along the ecliptic, while `ecl_short` (1yr) corresponds to the same, but with the short axis along (long axis perpendicular to) the ecliptic. These scenarios are neglected because their outages are time-correlated (see Fig. 9). `allsky` (poles) would be a scenario that observes in the manner of `allsky`, but only on the ecliptic poles as in `pole`.

We then compute the corresponding variance in incoming flux, and compare it to *TESS*’s noise budget, similar to the example in Fig. 7.

To evaluate the cumulative impact of Earth and Moon crossings on *TESS*’s Primary and Extended Missions we ask: for each camera, what fraction of the total observing time is *TESS* unable to operate at desired photometric precision because of Earth and Moon crossings?

An upper limit for what we mean by ‘unable to operate at desired photometric precision’ is when terrestrial or lunar flux make it impossible to observe a sizable portion of the stars in the *TESS* target star catalog with reasonable precision. Following our example of when the Moon is 24° from the camera boresight, the appended Fig. 26 shows that ∼50% of the stars that could be observed at sub-mmag precision over an hour no longer can. This of course depends on the target star catalog’s apparent magnitude distribution (Fig. 5), and the cutoff of ‘sub-mmag precision over an hour’ is arbitrarily selected.

Developing a detailed model of how these crossings impact *TESS*’s photometry is beyond the scope of this work. To account at least qualitatively for their effect in our simulation we adopt a simple approximation: we impose that a camera has an ‘outage’ if there are over $F_{\text{thresh}} \equiv 300 \text{ ct}/\text{px}/\text{s}$. This is roughly twice the maximal zodiacal background noise, which in our model ranges from 48–135 ct/px/s (see S+15 Sec 6.4.1). At an ecliptic latitude of 30°, Eq. 21

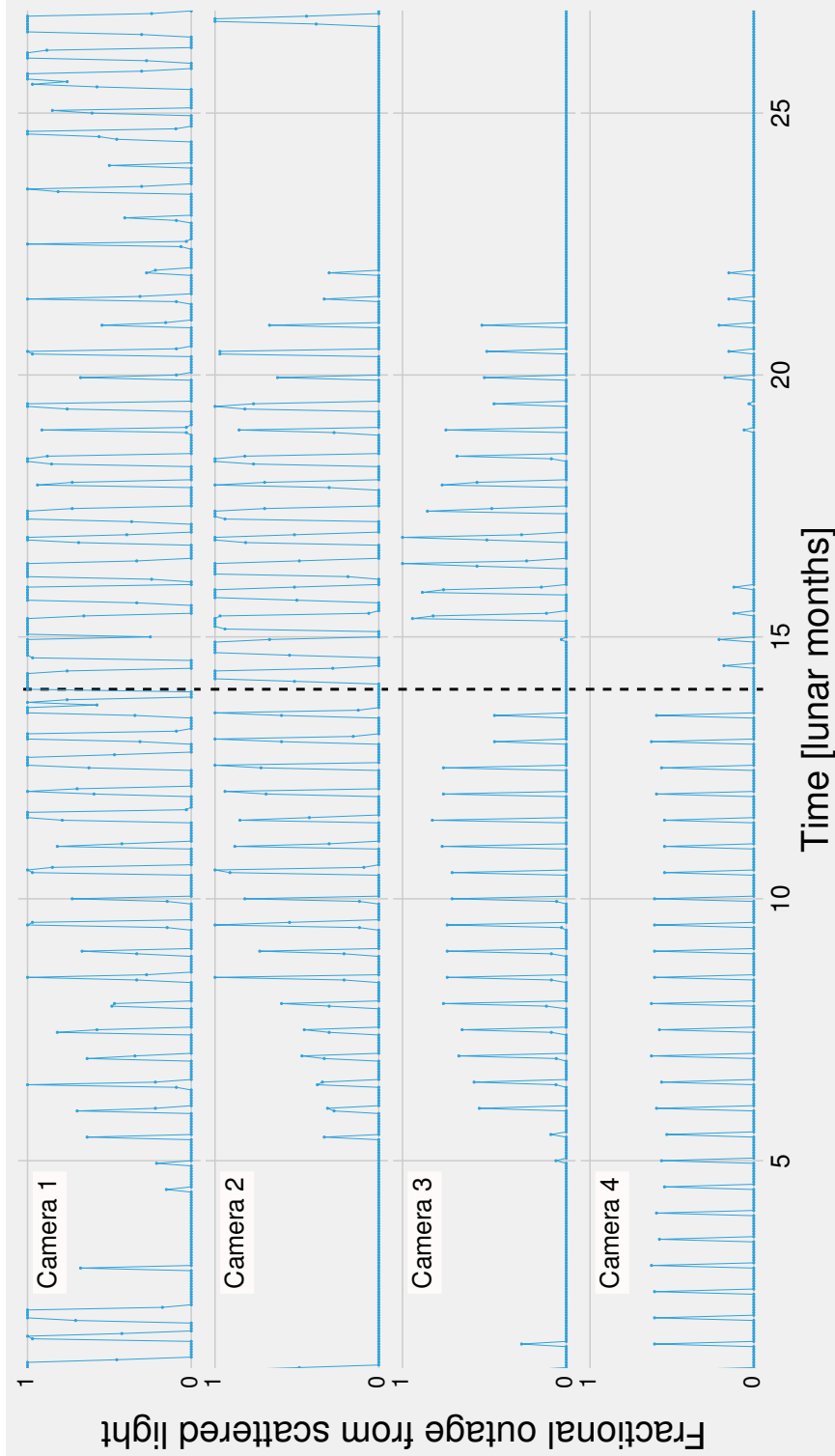


Figure 8: ‘Outage’ caused by direct and scattered Earthlight and Moonlight as a function of time in *TESS*’s orbit. Specifically, the y -axis shows the probability of having a polluted frame with mean incident flux $> 300 \text{ ct px}^{-1} \text{ s}^{-1}$ in a time-step bin of $1/20^{\text{th}}$ of an orbit (where the probability is the number of polluted frames divided by the total number of frames in that bin). The mean of this outage across any given year is used to compute the number of dropped fields in Table 1, which should then be an upper bound to the impact of Earth and Moon crossings. In this plot, the first year of observations are in the southern ecliptic hemisphere. The dashed line marks the beginning of ‘Year 2’ (northern hemisphere). *TESS* completes two orbits per lunar month. The worst fractional outage per orbit is in Camera 1, which points towards the ecliptic, over the first ~ 5 orbits of the second year. The plot has ‘spikes’ because outages only occur over a small fraction of *TESS*’s orbit when the relevant orbits align.

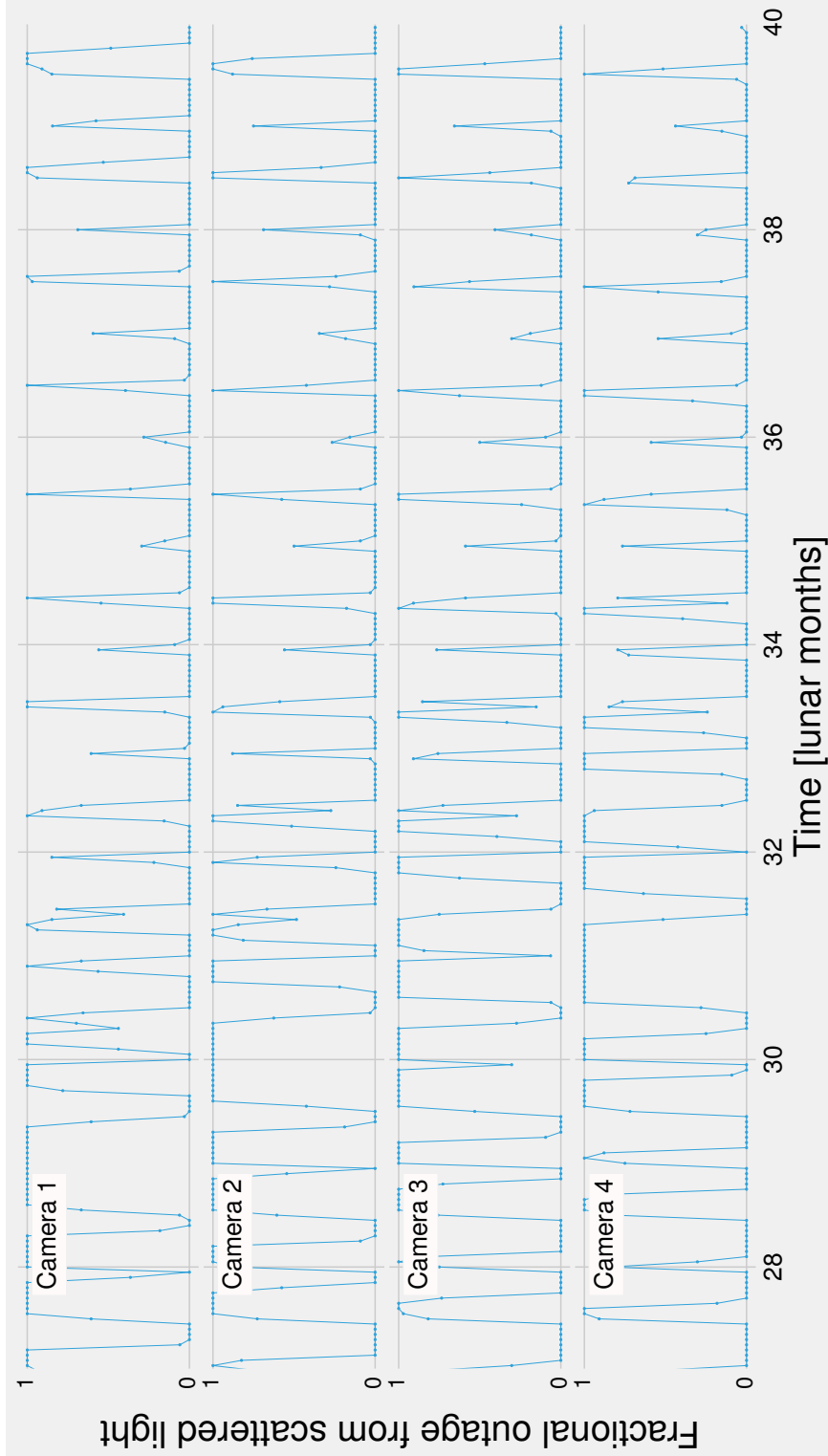


Figure 9: Same as Fig. 8, except showing a hypothetical third year in which TESS observes the ecliptic with the cameras' long axis along the ecliptic plane for the entire year. The latter half of the year experiences far less Earth and Moon interference than the first half. Considering it implausible that we would opt to sacrifice such a large fraction of our observing time, we study the `ecl_long` and `ecl_short` scenarios instead, as their observations avoid this effect during the first ~ 5 months.

of S+15 gives 75 ct/px/s, or about $F_{\text{thresh}}/4$.

We then compute the time-averaged fraction of each observing sector for which *TESS*'s cameras remain above this threshold. A given sector has ~ 660 hours of observing time over two spacecraft orbits. As an example, suppose that 220 of these hours had the Earth, the Moon, or both shining with a background flux $F > F_{\text{thresh}}$. This would correspond to a fractional outage of 1/3. We then compute the mean of this fractional outage across all 13 annual sectors to derive a 'mean camera outage' for each proposed pointing scenario. We then approximate the effect of Earth and Moon crossings by selectively omitting the closest integer number of observing sectors corresponding to the 'mean camera outage' described above. For instance, if the 'mean camera outage' was 17% of *TESS*'s observing time over a given year, we would omit the 2 (of 13) observing sectors that suffer the greatest number of lost hours, for that given camera. The relevant number of omitted sectors is shown in Table 1; an example of the resulting spatial distribution of detected planets is shown in Fig. 11.

As mentioned in Sec. 1.4, our planet detection simulation is not explicitly time-resolved; it takes the ecliptic coordinates of camera fields for each orbit as input to compute the observed baselines for each star in our galactic model. While our procedure ignores the temporal nature of the 'outages' (which is shown resolved over time-steps of 1/20th of an orbit in Figs. 8 and 9), it gives a sense of the cumulative impact of Earth and Moon crossings over the course of a year, which is sufficient for the purposes of this study.

The additional background corresponding to $F_{\text{thresh}} = 300$ ct/px/s becomes a noticeable noise source ($\gtrsim 1.5 \times$ lower precision) for targets with $I_c \gtrsim 12$ (cf. Fig. 7). This is roughly half of the target stars, with the greatest impact on the M dwarf sub-sample. By approximating all of the relevant time as an 'outage' lost across all stars (even for the bright ones for which the additional scatter is subsumed by other noise sources), our simulation results might be more sensitive to scattered light than *TESS* will be in reality. However, scattered light might have a non-Poisson component, and is expected to be non-uniformly distributed across each focal plane as the Moon or Earth moves relative to *TESS*'s pointing. This could make the effect worse than simulated.

The impact of this approximation on the planet yields of the Primary and Extended Missions are discussed in Secs. 2.1 and 2.3 respectively. The summarized result is that this model of Earth and Moon crossings leads to $\lesssim 10\%$ fewer $R_p < 4R_\oplus$ planet detections in the Primary Mission compared to the case of not accounting for the crossings at all. Detailed models of this process remain to be developed during the spacecraft's commissioning period.

1.7 Summary of Key Assumptions and Attributes of Planet Detection Simulations

- We focus almost exclusively on planets with $R_p < 4R_{\oplus}$.
- We assume the TRILEGAL catalog (modified to match interferometric radii, as described by S+15) is an accurate representation of the stellar neighborhood to $\lesssim 2\text{kpc}$.
- We omit the 5% of the sky closest to the galactic disk (see Fig. 4). We expect that *TESS*'s large pixel size ($21 \times 21''$) combined with crowding near the galactic disk will cause substantial source confusion and a large astrophysical false positive rate in this area. On a practical note, TRILEGAL cannot be queried within its run-time limit for some of these fields (cf. S+15 Sec 3.1).
- We assume prior knowledge of the radii and apparent magnitudes of TRILEGAL's synthetic stars, so we can prioritize the stars with a simple planet-detectability statistic (Eq. 3).⁸
- In evaluating a star's Merit (Eq. 3), we compute the apparent magnitude of each "star" based on the sum of the flux from the star itself as well as any companion or background stars (whose presence will not be known *a priori*).
- We use occurrence rates of planets as a function of radius and orbital period as calculated by Fressin et al. [2013] and Dressing and Charbonneau [2015]. We assume these are accurate for the $P \lesssim 180$ day planets to which *TESS* is sensitive. We note in passing that Burke et al. [2015] find slightly higher occurrence rates for planets orbiting GK dwarfs than Fressin et al. [2013].
- We assume the occurrence statistics of multiple-planet systems can be approximated with repeated independent draws from the single-planet distributions. We further assume the orbits of planets in multiple planet systems to be coplanar and stable (with period ratios of at least 1.2 between adjacent planetary orbits).
- For our instrument and noise models, we assume:
 - A point-spread function (PSF) derived from ray-tracing simulations. Compared with the PSF described by S+15 in their Sec 6.1, ours incorporates lower charge diffusion (based on laboratory measurements) and as-built (rather than ideal) optics. The net result is a slightly wider PSF, leading to 10% fewer $R_p < 4R_{\oplus}$ planets than the same PSF model used by S+15.
 - All stars are observed at the *center* of the *TESS* CCDs. This ignores off-axis and chromatic aberrations within the *TESS* optics, and consequently ignores the angular dependence of the pixel

⁸ Although it is difficult to determine accurate radii based on currently available data, we expect that by the time *TESS* launches *Gaia* will provide parallaxes and proper motions for many potential *TESS* targets, which will enable more reliable giant/dwarf discrimination and radius estimates.

response function (the fraction of light from a star that is collected by a given pixel). While S+15 attempted to model the field-angle dependence, we found some problems with this approach (see appendix Sec. C). Ignoring the field-angle dependence is a simplification that may lead to loss of accuracy, but since this applies uniformly to all the scenarios under consideration, it should still be possible to *compare* the results of different scenarios without much loss of accuracy.

- The time/frequency structure of all noise (except for stellar variability, see Eq. 2) is ‘white’. This means that we ignore time-correlated instrumental effects such as spacecraft jitter, thermal fluctuations, and mechanical flexure, which we expect will be at least partly mitigated by the mission’s data reduction pipeline.
- We assume the instruments perform equally well in year 3 as in years 1 and 2.
- The assumed contributors to white noise include: CCD read noise, shot noise from stars, a systematic noise floor of 60 ppm · hr^{1/2}, and zodiacal background. See Fig. 7 for the relative contributions of these terms as a function of apparent magnitude.
- The noise contributions from stellar intrinsic variability are assumed to be identical to those described by S+15 Sec3.5, which uses variability statistics from the *Kepler* data computed by Basri et al. [2013]. Unlike all previously mentioned noise sources, we do not scale noise from stellar variability as $t_{\text{obs}}^{-1/2}$, since the photon flux from stars may vary over time-scales similar to typical transit durations. Instead, we assume the noise contribution from stellar variability is independent across transits, and thus scales as $N_{\text{tra}}^{-1/2}$, for N_{tra} the number of observed transits.
- Our detection model is specified by Eq. 1. Specifically,
 - We require ≥ 2 transits for detection. We assume the period can be recovered without ambiguity and likewise there is no ambiguity in identifying which target star is exhibiting a given transit signal. We also assume a step-function detection threshold: for $\text{SNR}_{\text{phase-folded}} > 7.3$ and $N_{\text{tra}} \geq 2$, we rule transiting planets as detected, else they are not.
 - The top 2×10^5 Merit-ranked targets (Eq. 3) are observed at two-minute cadence, and the next 3.8×10^6 stars are observed at thirty-minute cadence. We use S+15 Sec. 6.8 approach to ‘blurring’ transits with durations $\lesssim 1\text{hr}$, so that for longer cadence images shorter transits get shallower depths and longer apparent durations. As described in Sec. 1.5, we verify that under this

assumption, our selection of PS stars is nearly complete for all detectable planets with $R_p < 4R_{\oplus}$, and it is highly incomplete for Jupiter-sized planets.

- We do not assume any prior knowledge of previous observations that may have been performed on our stars. For instance, observing the ecliptic, we do not account for *TESS-K2* overlap.
- For Earth and Moon crossings, we assume we can drop a fixed number of orbits of observing time for the cameras that suffer most from the Earth, the Moon, or both being in *TESS*'s camera fields. We summarize this effect in Table 1. Although this ignores the time-correlated nature of the outages shown in Figs. 8 and 9, it is sufficient for comparing detected planet yields across missions, and leads to $\lesssim 10\%$ fewer $R_p < 4R_{\oplus}$ planet detections compared to the case of not accounting for the crossings at all.
- We assume that we can (eventually) discriminate between astrophysical false positives (for instance background eclipsing binaries or hierarchical eclipsing binaries) and planet candidates.
- We can compute SNR with effective transit depth $\delta_{\text{dil}} = \delta \times D$ for $\delta = (R_p/R_{\star})^2$ the transit depth, and

$$D = \frac{\Gamma_T}{\Gamma_N + \Gamma_T} \quad (4)$$

where D is the dilution factor of a target star with incident photon flux Γ_T from the target star and incident photon flux Γ_N from neighboring stars (*i.e.*, background stars or binary companions).

The noise is computed by creating a synthetic image for every host star with a planet that transits above a ‘pre-dilution’ SNR threshold (this threshold is imposed for the sake of lowering our computational cost). This 16×16 pixel image is of the number of photoelectrons *TESS* sees from the star and its companions/background stars at each pixel of each CCD. We produce it through our PRF model, which in turn requires the host star’s T_{eff} and apparent I_c . Over each image, the noise is computed for a range of possible aperture sizes about the brightest pixel (see S+15 Secs. 6.2 and 6.3), and then finally a single ‘noise’ for each transit is selected by choosing the aperture size that minimizes the noise.

2 Planet Detection Statistics

Using the planet detection model described in Sec. 1.4 and the target selection procedure of Sec. 1.5, we simulate three years of *TESS* observing, for six different possibilities for the third year: `hemi`, `pole`, `hemi+ecl`, `ecl_long`, `ecl_short`, and `allsky`. How many new

planets do we detect, and how do their properties differ between Extended Missions?

2.1 Planet Yield from the Primary Mission

We first examine our results for just the Primary Mission – the first two years of *TESS*'s observing. We follow with an analysis of our detected planet populations from a single Year-3 Extended Mission (Sec. 2.2), and then all six of our proposed Extended Missions (Sec. 2.3). Here we highlight commonalities and differences between S+15 and this work.

Detected planet yield The first point of consideration is the detected planet yield, shown in Fig. 10. The number of Earths, super-Earths, and sub-Neptunes we detect agrees with the numbers quoted by S+15 to within 50%, despite the modifications described in Sec. 1.5 to the target selection procedure. Other changes to our simulation's assumptions, for instance using an as-built model of *TESS*'s PSF informed by laboratory tests (courtesy Deborah Woods) rather than the idealized PSF described in Sec 6.1 of S+15, had only minor impact on this final result (10% change in yield).

In the preparation of this report, a discrepancy emerged between our predicted ≈ 400 super-Earth detections and those shown in Fig. 18 of S+15, which displays ≈ 1400 planets. The subsequent investigation led to the discovery of a bug in the plotting script used to create Fig. 18 S+15 (an Erratum has been published). The error did not affect any of the results described in S+15's text, or the simulation results that were tabulated in the paper and sent electronically to interested parties. The corrected version of S+15's Fig. 18 shows ≈ 500 expected super-Earths, which closely agrees with our work when also accounting for the dilution error described below.

Another modification was the correction of a bug in the dilution calculations of S+15. A single missing symbol⁹ led S+15 to under-account for this effect. After correcting this error, the simulations yielded about 30% fewer Earth-sized and super-Earth planets than reported by S+15.

Properties of planets detected in Primary Mission We show the population properties of planets detected in postage stamps and full frame images during the Primary Mission in Figs. 12 and 13. In terms of the apparent planet radii R_p , orbital periods P , host star brightness, and host star T_{eff} , we qualitatively agree with the results of S+15 for the planets detected in postage stamps. For instance, the dearth of $P < 5$ day Neptune-radius ($R_p \lesssim 4R_{\oplus}$) planets in Fig. 12 was observed by

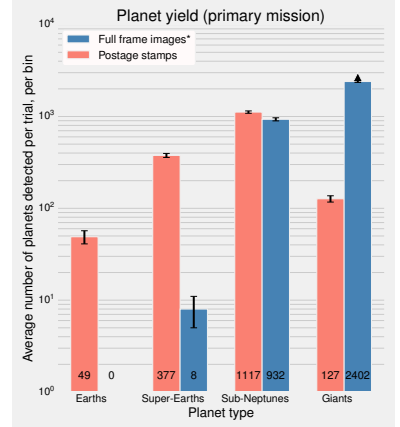


Figure 10: Mean numbers of planets detected in *TESS*'s Primary Mission. The number of Earths ($R_p < 1.25R_{\oplus}$), super-Earths ($1.25R_{\oplus} \leq R_p < 2R_{\oplus}$), sub-Neptunes ($2R_{\oplus} \leq R_p < 4R_{\oplus}$) and giants agree with the respective values quoted in Sullivan et al. [2015] to $\lesssim 50\%$. Our full frame images detections are complete for $R_p < 4R_{\oplus}$, and incomplete for giant ($R_p > 4R_{\oplus}$) planets, shown with a lower limit (see text for discussion). Error bars are from only Poisson fluctuations and do not account for systematic uncertainty.

⁹ An = rather than a +

Kepler [Mazeh et al., 2016], and thus it is present in our input occurrence rates, rather than being an observational bias. It was also seen by S+15.

The differences between planets detected in postage stamps vs. in full frame images follow our expectation from our Merit statistic. Namely, Fig. 13 shows that at a fixed brightness, full frame image detections tend to occur at larger stellar effective temperature (and thus stellar radius). At a fixed host star radius, postage stamp detections occur around brighter stars.

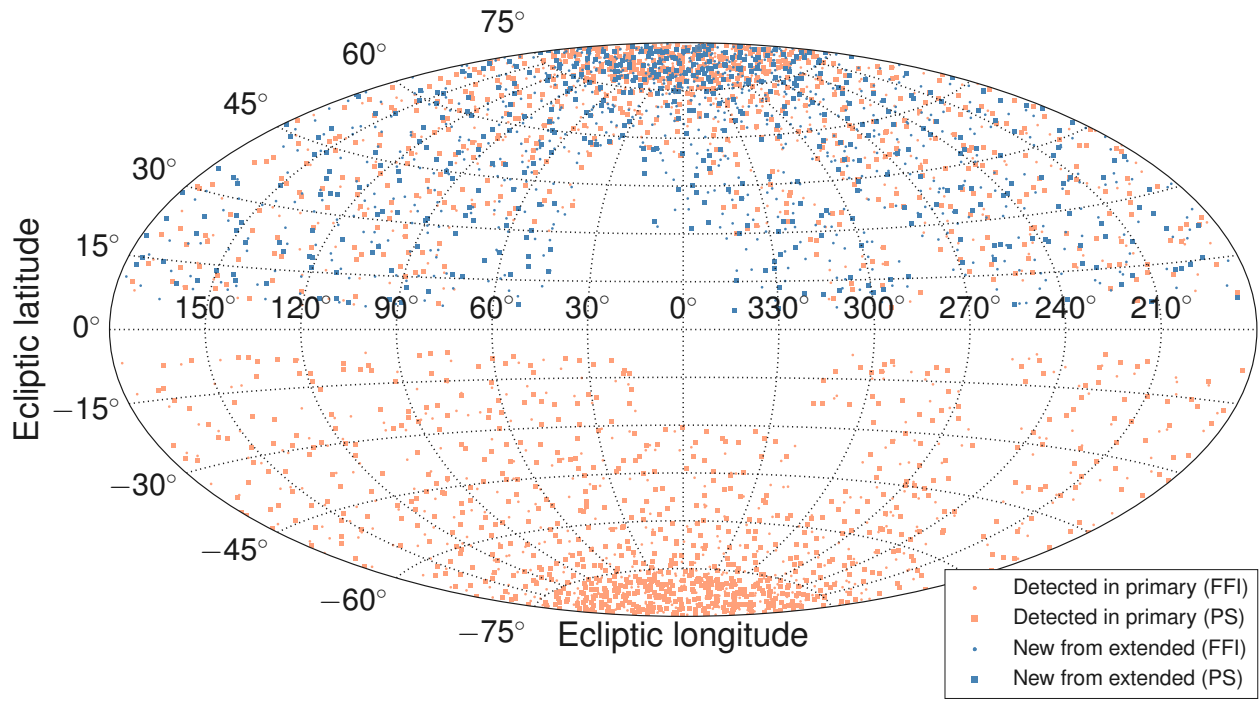
Impact of earth and moon crossings on Primary Mission’s detected planet yield During the Primary Mission, of the four cameras, Camera 1 (closest to the ecliptic) suffers the most from Earth and Moon crossings. As noted in Table 1, we remove 4 of its 13 ‘observing sectors’ from that year. This reduces the number of planet detections near the ecliptic, and is visible in the orange points of Fig. 11. In the Primary Mission *TESS* detects ~ 20 planets with $R_p < 4R_{\oplus}$ (PS+FFI) in each $24^\circ \times 24^\circ$ camera field nearest to the ecliptic. As implemented in our simulation, Earth and Moon crossings result in some fields simply not being observed, so in these cases planets orbiting stars in these fields are never detected. Considering only the Primary Mission, we would naively expect that dropping a total of 9 fields over the two years (again, see Table 1) would result in a loss of $\sim 9 \times 20 = 180$ planets. This agrees with what our simulations actually give: running them without accounting for Earth and Moon losses returns a mean of 2678 detected planets with $R_p < 4R_{\oplus}$, while running them with Earth and Moon crossings gives a mean of 2482 such planets (a loss of 196 planets; 7% of the $R_p < 4R_{\oplus}$ planet yield).

2.2 Planet Yield from Example Extended Mission: hemi

Before comparing our six selected Extended Mission scenarios simultaneously (Sec. 2.3), we describe the detected planet populations from a single realization of an Extended Mission. As an example case, we choose the hemi scenario.

A sky map showing the positions of detected planets for this mission is drawn in Fig. 11. Commenting on this map, we note that:

- Any planet detected following this scenario’s Primary Mission is also detected following its Extended Mission (using the combination of Primary & Extended datasets). We consequently color the detected planets depending on if they are discovered in the Primary Mission, or whether they are detected only by virtue of the extra data collected in the Extended Mission. In our simulation, these extra observations will lead to new detections (a) because



of an increased number of observed transits leading to a higher phase-folded SNR, which causes the transiting object's SNR to clear our threshold of 7.3, and/or (b) because raising the number of observed transits clears the minimum number of transits we require for detections ($N_{\text{tra}} \geq 2$).

- The ‘dropped’ fields described in Sec. 1.6 owing to Earth and Moon crossings are visible for both the Primary and Extended Missions in the $\lambda = (30^\circ, 0^\circ, 330^\circ, 300^\circ)$ fields.

In addition to examining the positions of the detected planets, we select and plot some of their key properties: planet radius R_p , orbital period P , apparent magnitude I_c , and effective temperature T_{eff} . See Figs. 12 and 13. Both of these figures are visualizations from a single Monte Carlo realization of the hemi scenario, and only show planets with $R_p < 4R_\oplus$. These plots clarify a few points:

- At a fixed period, Extended Missions help us detect smaller planets. At a fixed radius, Extended Missions let us probe out to longer periods. These are two important reasons to continue *TESS*'s observations.
- Nearly all $R_p < 2R_\oplus$ planets are detected in postage stamps, not

Figure 11: Positions of $R_p < 4R_\oplus$ planets detected in the hemi scenario. Squares (postage stamps) and dots (full frame images) are observed at 2 and 30 minute cadence respectively. Orange denotes detection over the first two years of observing (the Primary Mission), and blue denotes newly detected planets from the extra third year. The ‘gaps’ in fields due to Earth and Moon crossings during the Primary and Extended Missions are noted in Table 1. For instance, the field centered at $(\lambda = 330^\circ, \beta = 18^\circ)$ is observed in the Extended but not the Primary Mission.



full frame images. This is an indication that the top 2×10^5 Merit stars are a sufficient sample to detect nearly all of the $R_p < 2R_\oplus$ planets that *TESS* can detect over its first three years.

- Postage stamp detections are biased towards M dwarfs. Per Fig. 5, this is largely because our selection procedure chooses many M dwarfs.
- For a given effective temperature, the stars for which planets are detected in the full frame images are systematically fainter, compared to PS stars. Projecting the FFI detections onto apparent I_c magnitude (Fig. 13, right panel), the median brightness of stars with planets detected from FFIs is actually greater than the median brightness of planets detected from PSs. This is because our FFI sample has more bright large stars than the target star sample, since our selection procedure assigns higher Merit to dim M dwarfs than to dim K, G, or F dwarfs.

Figure 12: Radius vs period of detected $R_p < 4R_\oplus$ planets from one Monte Carlo realization of the hemi scenario. At a fixed period, Extended Missions help us detect smaller planets; at a fixed radius, they let us probe out to longer periods. The radius histogram, and the location of all dots (rather than squares) on the scatter plot show that almost all $R_p < 2R_\oplus$ planets are detected in postage stamps, not full frame images (also shown in Fig. 10).



There are a few other statistics that help quantify the value of this Extended Mission – how many new planets do we detect? How many are at long orbital periods? How many are in habitable zones? We respond to these questions in Sec. 2.3, in particular showing our detected planet yields in Fig. 14.

2.3 Comparing Planet Yields from all Extended Missions

To compare Extended Missions in terms of planet detection statistics, we focus on the subset of all detected planets that are *newly* detected from each Extended Mission. These may come from stars that were not observed at all in the Primary Mission (notably for scenarios such as `ec1_long`), or they may also come from transiting planets that were observed in the Primary Mission with $\text{SNR} < 7.3$, or from planets that were single-transiters in the Primary Mission (we require $N_{\text{tra}} \geq 2$) for detection. With this in mind, for each Extended Mission scenario we ask the following questions:

Figure 13: Apparent Cousins I magnitude plotted against effective temperature for $R_p < 4R_\oplus$ planets detected from one Monte Carlo realization of the `hemi` scenario. Postage stamp (PS) detections are biased towards M dwarfs in part because of our selection procedure. For a given effective temperature, full frame images (FFIs) are taken of dimmer stars.

1. N_{new} : How many new planets do we detect?
2. $N_{\text{new}, P>20\text{d}}$: How many of these new planets have periods > 20 days?
3. $N_{\text{new,HZ}}$: How many are in the habitable zone?
4. $N_{\text{sys,extra planets}}$: In how many systems in which at least one planet was detected during the Primary Mission do we find extra planets in the Extended Mission?
5. $N_{\text{new,atm}}$: How many new planets do we find that are amenable to atmospheric characterization (defined below by Eq. 5)?
6. $N_{\text{new,new stars}}$: How many of the new planets come from stars that were not observed in the Primary Mission?
7. $N_{\text{new,SNR}\vee N_{\text{tra}}}$: How many of the new planets come from candidates that after the Primary Mission had either a) $\text{SNR} < 7.3$ and/or b) less than 2 transits?

For each Year-3 scenario, we compare these numbers to the corresponding numbers from the Primary Mission as well as to the other 5 scenarios for Year 3. We show the results of our simulations in Fig. 14. The first point to notice is that for all but one of the new planet detection metrics (N_{new} , $N_{\text{new}, P>20\text{d}}$, $N_{\text{new,HZ}}$, $N_{\text{sys,extra planets}}$, $N_{\text{new,atm}}$, $N_{\text{new,SNR}\vee N_{\text{tra}}}$) the yields between Extended Missions vary by less than a factor of two. The exception is in $N_{\text{new,new stars}}$, in which `ec1_long` detects roughly twice as many planets orbiting never-before-observed stars as any other proposed mission.

The second point is on the absolute yields of new planets: postage stamp observations find $\mathcal{O}(500)$ new planets, relative to the Primary Mission's $\mathcal{O}(1500)$. Full frame image observations find $\mathcal{O}(800)$ new planets, relative to the Primary Mission's $\mathcal{O}(900)$. All Extended Missions find $\mathcal{O}(1300)$ new planets, relative to the Primary Mission's $\mathcal{O}(2500)$. We discuss these results – the rough invariance of the number of new planets to different pointing scenarios, and the essential contribution of FFIs – further in point #1 below.

Skimming the bottom panel for which missions are highlighted in green when accounting for both PSs and FFIs, we see that `pole` and `allsky` are the ‘superlative-winning’ missions in terms of detected planet statistics: considering both PSs and FFIs, `pole` places top-2 in 5 of 8 relevant categories, and `allsky` does the same in 6 of 8. They both do well at maximizing the number of newly detected planets, while also performing well at detecting long period planets, and thus planets in their stars’ habitable zones. `allsky` also has the largest number of systems in which extra planets are detected.

We now discuss each metric of Fig. 14 in more depth:

Target stars (2 min)	hemi	pole	hemi+ecl	ecl_long	ecl_short	allsky
N_{uniq}	2051	2219	2049	2114	2127	2130
N_{new}	499	616	489	530	472	584
N_{pri}	1544	1543	1540	1557	1552	1543
$N_{\text{new,P>20d}}$	137	153	127	118	108	176
$N_{\text{pri,P>20d}}$	214	210	215	216	215	216
$N_{\text{new,HZ}}$	102	108	100	95	94	128
$N_{\text{pri,HZ}}$	196	201	203	208	202	200
$N_{\text{sys,extra planets}}$	62	54	60	38	53	82
$N_{\text{new,atm}}$	11	7	15	19	21	17
$N_{\text{pri,atm}}$	97	102	100	99	104	98
$N_{\text{new,new stars}}$	29	37	50	193	110	20
$N_{\text{new,SNR}\vee N_{\text{tra}}}$	471	580	439	337	362	564

Full Frames (30 min)	hemi	pole	hemi+ecl	ecl_long	ecl_short	allsky
N_{uniq}	1716	1682	1782	1558	1574	1776
N_{new}	785	803	866	639	744	849
N_{pri}	940	939	936	947	933	931
$N_{\text{new,P>20d}}$	116	122	121	89	110	128
$N_{\text{pri,P>20d}}$	80	82	80	80	83	80
$N_{\text{new,HZ}}$	20	16	22	12	25	18
$N_{\text{pri,HZ}}$	9	8	9	9	8	9
$N_{\text{sys,extra planets}}$	9	7	10	5	7	10
$N_{\text{new,atm}}$	3	1	4	2	2	5
$N_{\text{pri,atm}}$	7	7	7	7	7	6
$N_{\text{new,new stars}}$	35	56	64	173	61	22
$N_{\text{new,SNR}\vee N_{\text{tra}}}$	750	747	802	466	682	827

Combined	hemi	pole	hemi+ecl	ecl_long	ecl_short	allsky
N_{uniq}	3767	3901	3831	3672	3701	3907
N_{new}	1284	1419	1355	1169	1216	1433
N_{pri}	2483	2482	2476	2504	2485	2474
$N_{\text{new,P>20d}}$	253	275	248	207	218	304
$N_{\text{pri,P>20d}}$	294	292	295	296	298	296
$N_{\text{new,HZ}}$	122	124	122	107	120	146
$N_{\text{pri,HZ}}$	205	210	212	217	210	208
$N_{\text{sys,extra planets}}$	71	65	70	44	61	92
$N_{\text{new,atm}}$	14	8	19	21	23	22
$N_{\text{pri,atm}}$	104	108	108	106	112	104
$N_{\text{new,new stars}}$	63	92	114	366	171	42
$N_{\text{new,SNR}\vee N_{\text{tra}}}$	1220	1327	1241	803	1045	1390

Figure 14: Detected planet metrics for six possible Extended Missions (values are means of 50 Monte Carlo realizations of our calculation, all for $R_p < 4R_{\oplus}$). Top: postage stamp detections, Middle: full frame image only detections, Bottom: sum of both. The best two scenarios for select statistics are bolded and highlighted in green.

N_{uniq} : number of unique planets detected over all 3 years. N_{new} : number of planets detected in year 3 that were not detected in years 1&2 (newly detected planets). N_{pri} : number of planets detected in the Primary Mission (years 1&2). $N_{\text{new,P>20d}}$: number of newly detected planets with orbital periods greater than 20 days. $N_{\text{pri,P>20d}}$: same as previous, but from the Primary Mission. $N_{\text{new,HZ}}$: number of newly detected planets satisfying $0.2 < S/S_{\oplus} < 2.0$ (approximate habitable zone). $N_{\text{pri,HZ}}$: same as previous, from the Primary Mission. $N_{\text{sys,extra planets}}$: number of systems in which extra planets are detected. $N_{\text{new,atm}}$: number of newly detected planets with SNR in transmission greater than (that of GJ 1214b)/2, as measured by JWST – see text. $N_{\text{pri,atm}}$: same as previous, from Primary Mission. $N_{\text{new,new stars}}$: number of newly detected planets that orbit stars that were not observed during the Primary Mission. $N_{\text{new,SNR}\vee N_{\text{tra}}}$: number of newly detected planets that were observed during the Primary Mission, but either (a) had $\text{SNR} < 7.3$ and/or b) had $N_{\text{tra}} < 2$, and so would not be ‘detected’.

1. N_{new} : we detect about as many new planets in Year 3 as we detect planets in either Years 1 or 2: roughly 1250. The worst and the best scenarios (ecl_long and allsky, respectively) differ only by a factor of 1.2. The fact that there are so many new planets to be detected from extended observations, particularly from full frame images, and that the absolute number of new planets does

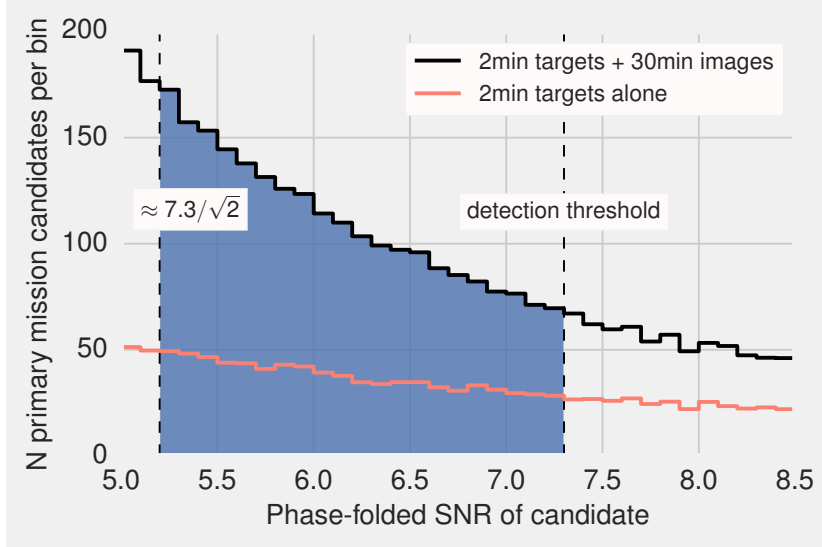


Figure 15: Histogram of phase-folded SNRs for candidate $R_p < 4R_{\oplus}$ planets following the Primary Mission (from both PS and FFI observations; values are means of 20 Monte Carlo trials; $N_{\text{tra}} \geq 2$). If an Extended Mission observes half of the sky, it roughly doubles the number of observed transits for half of the planets observed in the Primary Mission, enabling detection of $\approx 2316/2 = 1158$ planets (half of the blue integrated area in the plot). This coarse estimate is a similar result to our detailed calculations, and shows the value of continuing *TESS*'s observations irrespective of where we observe.

not depend strongly on the schedule of pointings, can be justified (post-facto) with Fig. 15. This figure illustrates a point that was originally noted by S+15: *TESS*'s Primary Mission will miss many short-period planets around bright stars, and is therefore incomplete even in its intended hunting ground. For stars with $I_c < 11$, there are $\sim 10\times$ more transiting $2 < R_p < 4R_{\oplus}$ planets on $P < 20$ day orbital periods than *TESS* will detect in its first two years¹⁰. S+15 similarly note that there are $\sim 20\times$ more transiting $R_p < 2R_{\oplus}$ ($P < 20$ day, $I_c < 11$ host star) planets in the sky than *TESS* will discover in its Primary Mission. Our findings agree: there are a substantial number of planets just below the detection threshold, predominantly with $2R_{\oplus} < R_p < 4R_{\oplus}$ (Fig. 10). An Extended Mission will probe and detect this population, in any of the scenarios we investigate. This result should hold equally well for realistic detection efficiency thresholds, and it demonstrates that extended observations will be valuable because *TESS* will not yet have detected all the planets in the parameter space of $R_p < 4R_{\oplus}$ planets orbiting bright stars on short-period orbits; there will still be small, short-period planets orbiting bright stars to be discovered after *TESS*'s Primary Mission.

2. $N_{\text{new}, P>20\text{d}}$: it will be possible to detect as many new $P > 20$ day planets in one year of *TESS*'s Extended Mission as in both years of the Primary Mission. The Primary Mission detects about 295 such planets; allsky and pole scenarios detect similar numbers. These two scenarios are achieving the goal of long-period planet detection in slightly different ways: pole maximizes the average

¹⁰ Fig 22 of S+15; only considers $R_{\star} < 1.5R_{\odot}$ stars

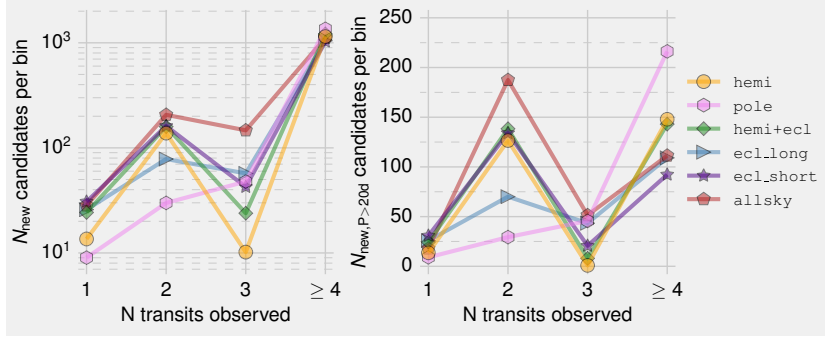


Figure 16: *Left:* Histogram of new $R_p < 4R_\oplus$ planet candidates from each Extended Mission as a function of the total number of observed transits over all 3 years. Planet candidates are ‘detected’ if $N_{\text{tra}} \geq 2$ (see Eq. 1). *Right:* Same as left, restricted to $P > 20$ day planets. If any given scenario has a ‘bump’ at 2 observed transits, then that scenario depends more heavily on our assumption of being able to make detections based on only two transits. Lines joining points have no physical meaning; they are intended to improve readability.

observing baseline per star, while `allsky` observes the greatest possible number of stars for longer than 40 days. The latter approach could succeed at detecting many planets (our result is that `allsky` detects the most $P > 20$ day planets), but it relies heavily upon the assumption that we can detect planets from only two transits over the course of the entire mission, even if this means only one transit in the Primary, and one transit in the Extended.

This point – that the ability of the `allsky` scenario to detect many long period planets is grounded on the assumption that two transits at high enough SNR are sufficient for detection – is made explicit in the right panel of Fig. 16. About half of the long period planets that `allsky` finds are detected with only two transits. By way of comparison, `pole` detects most of its long-period planets with ≥ 4 transits. This means that the `pole` detections are more secure. For two-transit detections, especially those separated by a gap of a year or more in the *TESS* data, it will be difficult to be confident in either the detection or in the derived orbital period. Experience from the *Kepler* mission showed that requiring 3 or more self-consistent transits substantially lowers the fraction of false signals [Burke et al., 2014]. If we restrict ‘detections’ to planets with both $N_{\text{tra}} \geq 3$ and $\text{SNR}_{\text{phase-folded}} \geq 7.3$, we find that `pole` detects ~ 260 new long-period planets, while the next-best scenarios, `allsky`, `hemi`, and `hemi+ecl`, all detect about 160.

3. $N_{\text{new,HZ}}$: we approximate the habitable zone as the geometric shell around a host star in which a planet’s insolation satisfies $0.2 > S/S_\oplus > 2.0$. With this approximation, the `allsky` scenario finds the most new habitable zone planets: 146 (which is subject to the same caveats discussed above for long period planet detections). The next-best scenarios, `pole`, `pole` and `hemi+ecl`, all detect around 120. Relative to the Primary Mission’s 210 detections, this means Extended Missions boost the number of detected habitable zone planets by a factor of ~ 1.6 . For purposes of weighing the

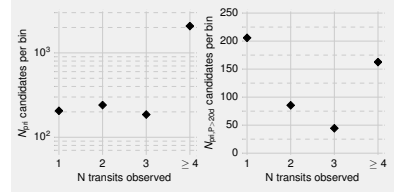


Figure 17: Similar to Fig. 16, but for the Primary Mission.

value of habitable-zone detections in deciding between missions, the result that these scenarios all detect a similar number of HZ planets indicates that this metric will likely not ‘tip the scales’ in any direction.

We note in passing that $\sim 80\%$ of the habitable zone planets that *TESS* detects orbit M dwarfs with spectral classes ranging from M4 - Mo, and $\sim 15\%$ of them orbit M dwarfs later than M4. We show the relevant cumulative distribution in Fig. 18. Additionally, our values for the number of $0.2 < S/S_{\oplus} < 2$ planets from the Primary Mission are slightly revised from those of S+15: while S+15 found 48 ± 7 planets with $0.2 < S/S_{\oplus} < 2$ and $R_p < 2R_{\oplus}$, we find 34 ± 5 such planets. Adopting the habitable zone of Kopparapu et al. [2013], S+15 found 14 ± 4 planets with $R_p < 2R_{\oplus}$. We find 11 ± 3 such planets. The rule of thumb that Extended Missions give roughly $1.6 \times$ the number of new $0.2 < S/S_{\oplus} < 2$ habitable zone planets applies to the Kopparapu et al. [2013] habitable zone as well as $0.2 < S/S_{\oplus} < 2.0$. Another point raised by Fig. 19 is that the Kopparapu et al. [2013] habitable zone, which is physically motivated by 1-D radiative-convective cloud-free climate models with accurate absorption coefficients, results in roughly 3 times fewer ‘habitable zone’ planet detections than our ad-hoc criterion of $0.2 < S/S_{\oplus} < 2$.

4. $N_{\text{sys,extra planets}}$: for how many systems do we detect extra planets? Our assumptions about multiple planet system distributions are crude – we assume independent probability draws from single planet occurrence distributions. Thus our simulated planet population may not have systems of tightly packed inner planets in realistic numbers. That said, we expect this statistic to be some indication of the information that we are not explicitly modeling, but which can be obtained from extended observations of planetary systems post-planet detection. This additional information includes improved precision on physical and dynamical parameters of the system. It also includes transit timing variations, which could be used to discover non-transiting planets as well as transiting outer companions. TTVs can also give dynamical hints for the formation history of planetary systems, for instance, discriminating between *in situ* formation and inward migration as Mills et al. [2016] argued for the Kepler 223 system.

The most prominent feature in the results for this metric is that `ec1_long` detects the fewest systems with extra planets (44, which is 39% worse than the next-best). This is reasonable because `ec1_long` spends the most time looking at new sky, and in the process observes fewer systems that were detected in the Primary Mission. `hemi`, `hemi+ecl`, `pole`, and `ecl_short` all perform simi-

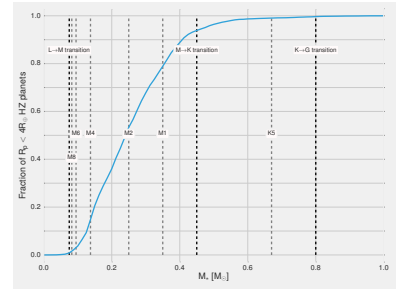


Figure 18: Cumulative distribution of $R_p < 4R_{\oplus}$ and $0.2 < S/S_{\oplus} < 2$ planet candidates from the Primary Mission (a proxy for the habitable zone). Boundaries of spectral classes are highly approximate, and taken from Habets and Heintze [1981] and Baraffe and Chabrier [1996].

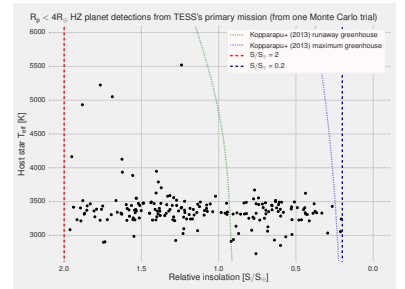


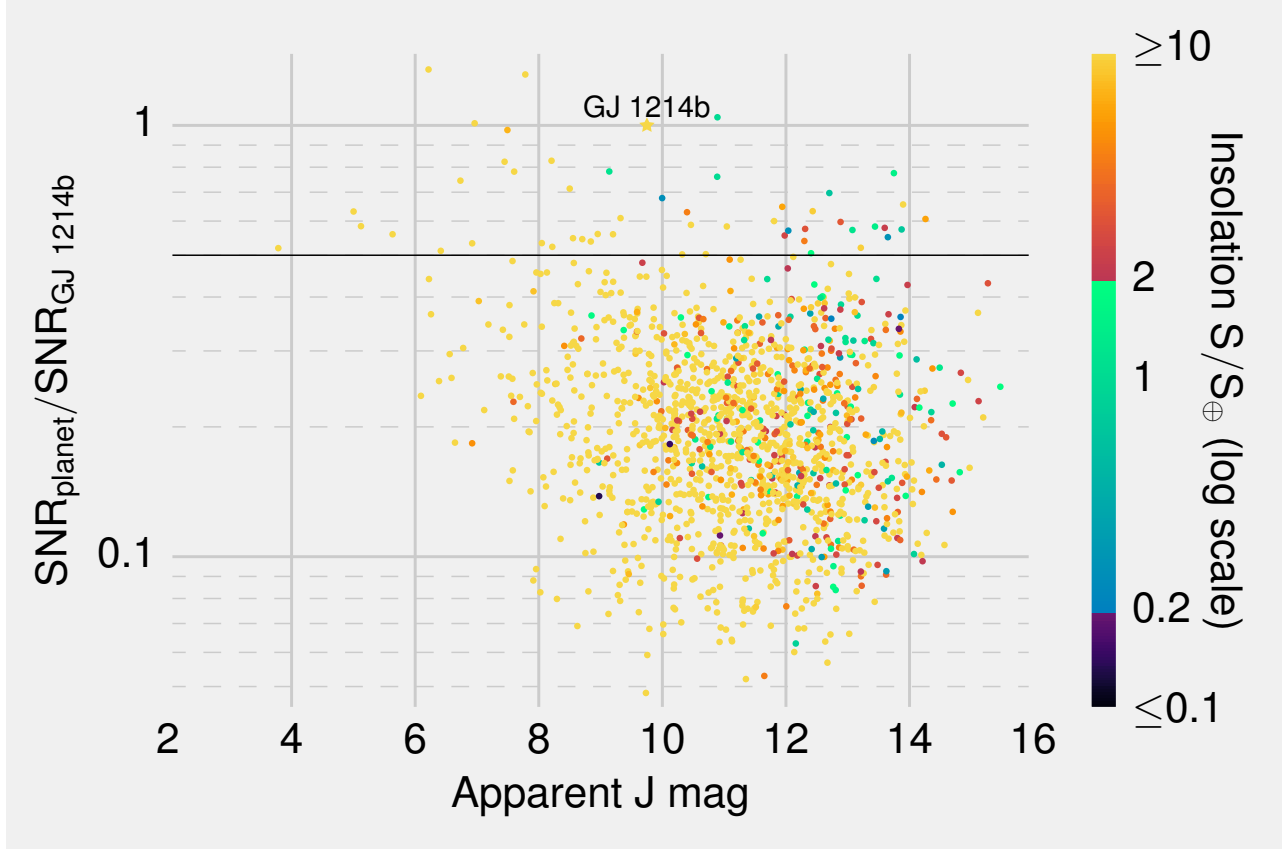
Figure 19: Scatter plot of $R_p < 4R_{\oplus}$ planet candidates falling in the S+15 or Kopparapu et al. [2013] habitable zones.

larly, detecting ~ 65 such planets. `allsky` detects the most, at 92. While this is still subject to the assumption of two-transit recoverability, in this case the requirement is not too strong: only 10 of `allsky`'s systems with newly detected planets come from the case where the extra detected planet comes from two transits.

5. $N_{\text{new,atm}}$: We define ‘planets that are amenable to atmospheric characterization’ to mean planets whose SNR in transmission is at least half as large as that of GJ 1214b. We chose “at least half as large” rather than “equal to” in order to give a sufficiently large sample to prevent Poisson fluctuations from hindering our comparisons. The relevant signal in transmission spectroscopy is the ratio of the areas of atmosphere’s annulus to the star’s disk on the sky plane, $\delta_{\text{atm}} = 2\pi R_p h_{\text{eff}} / (\pi R_\star^2)$, where the effective scale height of the atmosphere h_{eff} is proportional to the actual scale height. Assuming that the planet is in thermal equilibrium with incident radiation from the host star, and that its atmosphere has known mean molecular weight and Bond albedo, we can compute a representative signal. The noise performance depends on the observing instrument, and could be complex if not simply dominated by shot-noise from IR photons. We circumvent such complexities via an empirical formula provided to us by Drake Deming, based on a multi-variate regression fit to detailed simulations performed by Dana Louie. This formula estimates the SNR in transmission from 4 transits observed with *JWST*’s NIRISS instrument:

$$\begin{aligned} \log_{10} \text{SNR} = & 2.98 \log_{10} \left(\frac{R_p}{R_\oplus} \right) - 1.019 \log_{10} \left(\frac{M_p}{M_\oplus} \right) \\ & - 1.459 \log_{10} \left(\frac{R_\star}{R_\odot} \right) - 0.249 \log_{10} \left(\frac{a}{\text{AU}} \right) \\ & - 0.147(V - 5.0) + 0.193 \end{aligned} \quad (5)$$

for V the host star’s apparent V -band magnitude (calibrated for $3 > V > 22$), R_p the planet radius, M_p the planet mass, R_\star the star radius, and a the planet’s semi-major axis. The coefficients are physically sensible: the 2.98 coefficient of R_p minus the 1.019 coefficient of M_p implies that the SNR depends inversely as bulk density, with puffier planets giving higher SNR for transit spectroscopy. Although this formula uses a V band magnitude ($\approx 0.5\text{--}0.6\mu\text{m}$), while NIRISS’s SOSS mode covers $0.6\text{--}2.8\mu\text{m}$, the only difference if we were to use J band magnitudes would be in the coefficients preceding the stellar radius and the semi-major axis terms (and thus implicitly, in the stellar mass). Focusing our analysis to a SNR measured by *JWST* is sensible given *TESS*’s role as a ‘*JWST* finder scope’ [Deming et al., 2009]. We focus specifically on NIRISS but our analysis will be broadly applicable to other *JWST*



instruments for transmission spectroscopy (see review by Beichman et al. [2014]).

The system values for GJ 1214b are those found by Charbonneau et al. [2009]: $R_p = 2.678R_\oplus$, $M_p = 6.55M_\oplus$, $R_\star = 0.211R_\odot$, $a = 0.0144\text{AU}$, $V = 15.1$. Using Eq. 5, we compute the SNR in transmission for all detected planets, for all Extended Mission scenarios. We normalize them to the equivalent SNR for GJ 1214b (3.94, per Eq. 5). Fig. 20 shows one realization of the resulting distribution for planets detected in all three years of the pole scenario.

TESS mostly detects strongly irradiated planets (most points on Fig. 20 are yellow). A very small number, $\lesssim 10$, are both in the approximate habitable zone and also ‘favorable for atmospheric characterization’. Of course, a highly compelling target with lower SNR in transmission per transit might merit a more ambitious *JWST* observing program. We note that all of these planets are assumed to have identical mean molecular weights and cloud properties.

Figure 20: Scatter plot showing the SNR in transmission of detected planets with $R_p < 4R_\oplus$ from one Monte Carlo realization of all 3 years of the pole scenario. The SNR is computed from Eq. 5. Planets above the horizontal black line ($\text{SNR}_{\text{planet}}/\text{SNR}_{\text{GJ } 1214\text{b}} = 0.5$) are counted for Fig. 14’s metric of planets with ‘good’ atmospheres for transmission spectroscopy. GJ 1214b is marked with a star. The coloring of planets indicates their relative insolation, as well as whether they are in our approximate habitable zone ($0.2 < S/S_\oplus < 2$).

More importantly, Fig. 14 shows that most of the planets with atmospheres that are best for transmission spectroscopy are already discovered after two years. The best Extended Missions (`hemi+ecl`, `ecl_long`, `ecl_short` and `allsky`) boost the yield of such planets from ~ 100 ($N_{\text{pri,atm}}$) to ~ 120 ($N_{\text{pri,atm}} + N_{\text{new,atm}}$). The worst, `pole`, finds about an additional 10. This best-case boost of $1.25 \times$ more ‘good’ planets for atmospheric characterization is less than the relative boost of $1.6 \times$ more newly detected long period planets. Put differently, among the various possibilities for the Extended Mission, there is more variation in $N_{\text{new,P>20d}}$ than in $N_{\text{new,atm}}$.

6. $N_{\text{new,new stars}}$: Intuitively we expect that to maximize the number of planets detected around “new” stars (those which were not observed during the Primary Mission) we should collect as many photons as possible from new stars. And the region on the sky with the greatest number of new stars is the ecliptic. It is not surprising, then, that the `ecl_long` scenario finds the largest number of planets around new stars. The `ecl_long` scenario dedicates 7 of a single year’s 13 observing sectors to the ecliptic (where the other 6 are spent centered at the North Ecliptic Pole due to excessive Earth and Moon crossings). It consequently detects twice as many new planets about newly observed stars as the next-best scenarios: `ecl_short` and `hemi+ecl` (366 vs 171 and 114, respectively). These latter two scenarios also spend time observing the ecliptic, but with only one camera, rather than with all four cameras simultaneously. We note that even though `ecl_long` is the scenario most successful in detecting planets about new stars, the new stars represent only $\sim 30\%$ of the total number of new detections.¹¹
7. $N_{\text{new,SNR}\vee N_{\text{tra}}}$: This statistic is the number of newly detected planets that are detected either (a) due to their final SNR clearing our threshold (logical) or (b) their number of observed transits being greater than or equal to 2. It is the complement to $N_{\text{new,new stars}}$: scenarios like `hemi`, `pole`, and `allsky` that do not observe many new stars will detect all of their planets from a boosted SNR and/or clearing the minimum transit threshold.

Comment on meaning of ‘detected in postage stamps’ vs ‘detected in FFIs’
The invested reader may inquire “what about the cross-over case of planets that are observed as PSs during the Primary (Extended) Mission, but as FFIs in the Extended (Primary) Mission? These are not explicitly listed in Fig. 14”. When describing the entire unique planet population detected from Years 1-3, for simplicity of language we use ‘postage stamp detections’ to refer to planets that are observed

¹¹ Here, we remind the reader that “new” refers only to *TESS* observations. Some of these stars will have been observed by *K2* or other projects (see discussion in Sec. 3).

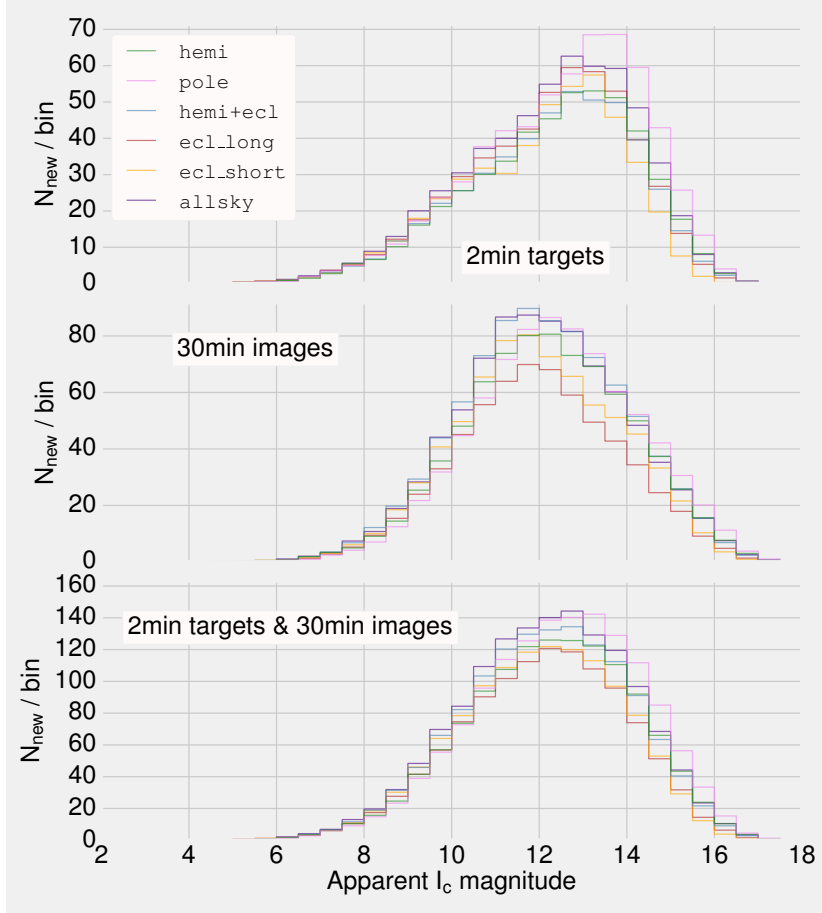


Figure 21: Histogram of apparent I_c magnitude of host star for newly detected $R_p < 4R_\oplus$ planets from all Extended Mission scenarios, for top: postage stamp detections, middle: full frame image detections, bottom: the sums thereof. While pole does well by most metrics, a larger proportion of the new planets it detects orbit dim stars compared to alternatives like allsky or hemi+ecl.

at any time (Primary or Extended Missions) at 2 minute cadence. In these cases, the dominant contribution to the final signal to noise ratio tends to come from the PS observations. When describing new planet detections, we use ‘postage stamp detections’ to mean planets that were newly detected due to being observed as postage stamps in the Extended Mission. In other words, this ‘cross-over’ point only matters in discussions of the unique planet population from an entire mission, Years 1-3. Considering just the newly detected planet population, we can unambiguously specify whether the new detections came from full frame images or postage stamps, irrespective of their observations from the Primary Mission.

2.4 On the Brightness of Stars with Detected Planets

While pole does well by most metrics, a larger proportion of its newly detected planets orbit dimmer stars than the planet populations detected from alternatives like allsky or hemi+ecl. We demon-

strate this in Fig. 21. The main point here is that if our only priority were to maximize the number of new detections around bright host stars, then `pole` would be the worst among the scenarios considered here. For instance, arbitrarily setting the bound at $I_c < 10$ and numerically integrating from Fig. 21’s data, we see in Table 2 that there is a $\sim 30\%$ difference between the missions. For point of reference, the Primary Mission detects 386 such planets – so a single year of Extended Mission detects roughly as many planets orbiting bright hosts as a single year of Primary Mission.

hemi	pole	hemi+ecl	ecl_long	ecl_short	allsky
162	154	188	167	183	198

3 Discussion

3.1 Planning Year 3 with Years 4–N in mind

TESS’s orbit is stable, in principle, for more than 1000 years [Gangestad et al., 2013]. While minor mechanical failures should be expected on the timescale of a few years, it is plausible that the spacecraft could be operable for up to a decade. Therefore, when choosing any particular plan for a one-year Extended Mission, it makes sense to also consider the implications of an even longer Extended Mission.

A simple point is that `hemi`, `pole`, and `hemi+ecl` can all be inverted to their southern or northern complements for a fourth year of observing. This will yield a comparable number of new planets to what they find in year 3 ($\mathcal{O}(1300)$ with $R_p < 4R_{\oplus}$). This would continue *TESS*’s role as a planet-discovery machine, while also addressing the matter of refining ephemerides in order to enable detailed characterization with suitable instruments.

While our simulations show that observing opposite hemispheres in Years 3 and 4 leads to many planet detections, we have not compared this strategy with observing the same hemisphere in both years (e.g., performing `hemi` in both Years 3 and 4). The latter approach might improve planet detection statistics, in particular with small and long-period planets. An argument against such a strategy would be that it postpones refining the *TESS* planet ephemerides until Year 5. We leave the detailed comparison for future work.

In terms of the other strategies, `ecl_long`, `ecl_short`, and `allsky` are less obviously extensible to multiple years. The main reasons to return to the ecliptic after performing `ecl_long` or `ecl_short` would be to make *TESS*’s survey truly ‘all-sky’, and to perform *K2* follow-up observations (see discussion below). Of course, this would need to happen during intervals in which the Moon and Earth were not in

Table 2: Number of new, $I_c < 10$, $R_p < 4R_{\oplus}$ planets from each Extended Mission (average of 50 Monte Carlo realizations of our code; showing sum of PSs & FFIs). `pole` detects the fewest new planets orbiting bright stars.

the way. `hemi+ecl` would also achieve this goal.

Any of our proposed scenarios could simply be repeated indefinitely, as could possible two-year Extended Missions in which our scenarios would be followed by their respective complement hemispheres. However, qualitatively novel trade-offs may arise when comparing two-year Extended Missions. For instance, after completing the Primary Mission, compare the 2-year extension scenarios of #1) two years of `allsky` vs. #2) repeating the Primary Mission for two years. If we repeat the Primary Mission over 2 years, the northern and southern CVZs get 1 additional year each of continuous observation. If we execute `allsky` for 2 years, the northern and southern ‘long viewing zones’ each get 2 years of 14-day windowed observations. While each CVZ star receives the same total observing time, CVZ stars in #1 have a 1-year baseline, continuously sampled, while those in #2 have a 2-year baseline, half-sampled. Thus #2 allows 2-transit detections of $P \lesssim 1$ year planets over 2% of the sky. #1 allows 2-transit detections of $P \lesssim 6$ month planets over 1% of the sky. In the competition between better time-sampling and longer baselines, it is not clear which strategy is superior.

Another longer-term question is “when will *TESS* hit the point of diminishing returns?” The ‘low-hanging fruit’ of small planets transiting bright stars at short orbital periods will become “picked over” if *TESS* observes the same sky indefinitely. The most important qualitative point of this memo, made in Fig. 15, is that after *TESS*’s Primary Mission there will be many objects remaining for which merely doubling the number of observed transits will enable their detection. Eventually though, once *TESS* is complete for $R_p < 4R_\oplus$ planets orbiting bright stars on $P < 20$ day orbits, more observations will only allow us to probe out to longer orbital periods and dimmer stars. We have not yet quantified when *TESS* will reach this regime.

3.2 The Ephemeris Problem

Analytic motivation For follow-up observations, we will often need to predict future times of transits or occultations, ideally with an accuracy of an hour or less. After enough time has passed that the uncertainty has grown to an operationally significant value, we say that the ephemeris has gone “stale,” *i.e.*, it presents a major obstacle to many follow-up programs. For *TESS*’s ground-based follow-up campaign, following up a planet with a stale ephemeris would require much more observing time for a successful result. Likewise, for planning space-based observations, for which observing time is always scarce, it is extremely important to have a reliable and precise

ephemeris. For mass determination through the Doppler method, a stale transit ephemeris adds uncertainty to the planetary mass measurements, by increasing the number of effectively free parameters.

Consider then the problem of estimating $\sigma_{t_c}(T_x)$, the uncertainty of the mid-transit time σ_{t_c} for a given planet at some time T_x following its last-observed transit. We begin analytically: assume that the planet has $N_{\text{tra}} = 2$ observed transits, spaced an orbital period $P = 14$ days apart. Because that period is one half the nominal *TESS* dwell time of a given pointing, it represents the shortest period for which typically $N_{\text{tra}} = 2$, and as such is the worst-case scenario for predicting the times of future transits, amongst cases with $N_{\text{tra}} > 1$. Given two mid-transit times, each measured with the time's uncertainty σ_0 , separated by P , the uncertainty of a future mid-transit time can be derived by standard least-squares fitting and propagation of errors (e.g. Lyons [1991], Equation 2.18):

$$\sigma_{t_c}(T_x) = \sigma_0 \sqrt{1 + 2T_x/P + 2(T_x/P)^2} \quad (6)$$

Note that for observing future transits, $E \equiv T_x/P$ is a positive integer, and the above equation can be re-expressed:

$$\sigma_{t_c}(E) = \sigma_0 \sqrt{1 + 2E + 2E^2}, \quad (7)$$

which is bounded by the simpler approximation:

$$\sigma_{t_c}(E) \lesssim \sigma_0 (1 + \sqrt{2}E), \quad (8)$$

which is exact at $E = 0$, has a maximum 8% fractional error at $E = 1$, and becomes increasingly accurate as E increases. By $E = 20$, the fractional error of the latter approximation is less than 1%.

At 2-minute cadence, a typical value for the per-transit timing uncertainty is $\sigma_0 = 4$ minutes. For example, if $T_x = 2$ years and $P = 2$ weeks, then $E \approx 50$, so $\sigma_{t_c} \approx 75\sigma_0$. Hence the predicted 1σ uncertainty on its mid-transit time is 5 hours (two years later) or 10 hours (four years later).

This leads to a simple rule of thumb:

For a two-transit super-Earth, the 1σ uncertainty in the predicted transit time, in hours, is numerically equal to about $2Y$, where Y is the number of years after the Primary Mission.

If the transits are observed only at 30-minute cadence, then uncertainty will be roughly 4 times greater: $\sigma_0 \sim 16$ minutes. This claim ("4× greater") is based on Figure 9 of [Price and Rogers, 2014], a plot of the effects of finite cadence on timing precision. We compared the precisions of 2-min and 30-min cadences for their specific example of $P = 10$ days and a dwell time of 1 month.

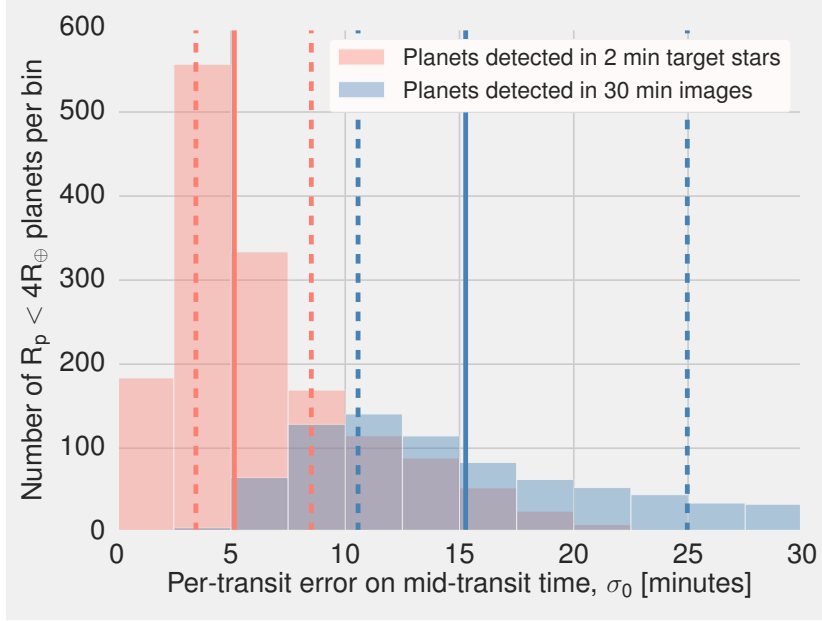


Figure 22: Uncertainty of mid-transit time on a single transit, σ_{tc} , for all detected $R_p < 4R_\oplus$ planets from the Primary Mission as computed from Eq. 10. Solid lines are medians, dashed lines are 25th and 75th percentiles.

On the other hand, Fig. 17 shows that 7 in 8 of the planets detected by *TESS*'s Primary Mission will have $N_{tra} > 3$ and so their ephemerides should be better than the worst case example derived analytically above. Rather than generalize the analytic equations, we resort to numerical simulations in order to predict the uncertainties of mid-transit times for planets expected to be discovered by *TESS*'s Primary Mission.

Numerical analysis We start with the analytic form Price and Rogers [2014] derive for the per-transit uncertainty on the mid-transit time σ_0 :

$$\sigma_0 = \frac{1}{Q} \sqrt{\frac{\tau T}{2}} \left(1 - \frac{t}{3\tau}\right)^{-1/2} \quad (9)$$

when $\tau \geq t$ and

$$\sigma_0 = \frac{1}{Q} \sqrt{\frac{t T}{2}} \left(1 - \frac{\tau}{3t}\right)^{-1/2} \quad (10)$$

when $t > \tau$, where Q is the SNR per transit, t is the cadence, T is the transit duration, and τ is the ingress (or egress) time. We have all the latter terms from our yield simulation, and show the resulting distribution of σ_0 in Fig. 22. Indeed, our suggested σ_0 of about 4 minutes for postage stamps and 16 minutes for full frame images is reasonable, which is good because we computed the former from the $t \rightarrow 0$ limit of Eq. 9 originally derived by Carter et al. [2008].

Given the distributions on per-transit uncertainty of t_c , we then took an example planet with 4 transits. We drew "observed" mid-

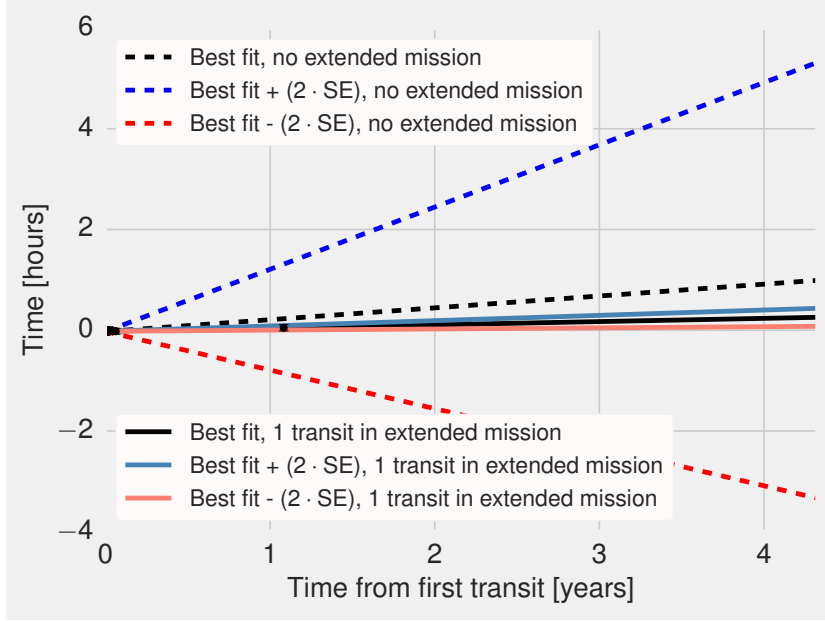


Figure 23: Observed mid-transit times (dots) and best fits to a linear ephemeris (lines). The dashed lines fit 4 data points from a nominal planet. The solid lines do the same, but with an additional transit observed one year later. ‘SE’ is the standard error on the slope which multiplied by 1.96 (rounded to 2 in the legend) gives a 95% confidence interval between the blue and orange lines.

transit times from a Gaussian with zero mean and standard deviation σ_0 , and then ran a linear least squares regression. We then added just one data point 1 year after the final observed transit, and repeated the regression. This produces a cartoon-plot, Fig. 23, which confirms two expected points:

1. Years after the initial discovery, the uncertainty of mid-transit time is of order hours.
2. If we detect an additional transit 1 year after the final observed transit from the Primary Mission, the uncertainty on the mid-transit time decreases by an order of magnitude.

We proceed by repeating the above procedure for every planet, and evaluate typical 95% confidence intervals (“uncertainties”, loosely) for t_c , at typical times after the first transits, for all of our detected planets. Specifically, we take them at $T_x = 2$ and 4 years, and get Fig. 24. This figure confirms (top left panel) our analytic expectation that the uncertainty of mid-transit times in hours should be somewhat less than twice the number of years after TESS first observes the planet at 2-min cadence, since most such planets have $N_{\text{tra}} \geq 4$. It also confirms our rough expectation that the uncertainty on FFI mid-transit times is roughly 4 times that of postage stamps, although the uncertainties on FFIs have a much broader tail than PSs.

More importantly, Fig. 24 emphasizes the importance of refining TESS’s ephemerides: if we do not, the typical TESS planet will have



many hours of uncertainty on its mid-transit time a few years following its detection. If we do follow-up with an Extended Mission, we will be able to predict when the planet transits to $\lesssim 1$ hour for many more years. This argues strongly for an Extended Mission which, whether over 1 or 2 years, re-observes many if not all of the targets that *TESS* detects in its Primary Mission. The smallest-radius Earths and super-Earths may otherwise be much more difficult to follow up.

3.3 Risks and Caveats

Risk that planet detection simulation gets yield wrong: What is the risk that we over or under-estimated *TESS*'s planet yield, either in the Primary Mission, or in any given Extended Mission? We summarized the assumptions that went into our yield calculations in Sec. 1.7. We made them believing that they were all good enough for useful relative comparisons of different sky-scanning scenarios, even if they

Figure 24: Top row: histogram of 95% confidence intervals 2 (left) and 4 (right) years following the first detected transit in the Primary Mission. 20 minute bins. Bottom row: histogram of 95% confidence intervals 2 (left) and 4 (right) years following the first detected transit in the Primary Mission, but with an additional data point added to the analog of Fig. 23 one year after the transit in the initial time series (5 minute bins). Note that the top row's timescale is an order of magnitude greater than the bottom row. Solid lines are medians, dashed lines are 25th and 75th percentiles.

are not correct in absolute terms to better than $\approx 50\%$.

Highlighting a few of these assumptions, in order of what we feel is decreasing concern:

- 1.) We assume no knowledge of the outcomes of prior transit searches.

As indicated in the text, this assumption is worst for the `ecl_long` and `ecl_short` scenarios, for which $K2$ and *TESS*'s overlap will be important. Estimating the magnitude of our error, assume $K2$ will have observed 70% of the sky in the $|\beta| < 6^\circ$ band about the ecliptic by 2019. Of the 1169 'new' $R_p < 4R_\oplus$ planets that *TESS* detects in `ecl_long`, 239 of them are within $|\beta| < 6^\circ$ of the ecliptic, and thus roughly 167 will already have been observed by $K2$ (assuming the same stars were selected in $K2$ observations). This simple estimate quantifies our global error in reporting 'new' planets near the ecliptic ($\sim 15\%$ will not be truly 'new'), but neglects the issue of merging the two datasets to discover long period planets. This latter opportunity could be an important reason to actually do `ecl_long` or `ecl_short` and thus demands detailed study, which we recommend below.

- 2.) We use a SNR threshold of 7.3. This number was computed by S+15 based on the argument that it would be a sufficient threshold to give one statistical false positive per 2×10^5 light curves. Applying the same criterion to full frame images would lead to more than one false positive, since full frame images come from a much larger sample of stars. Any pipeline that is written to work with *TESS* data will confront this problem: processing 10^8 vs. 10^6 stars requires different false positive thresholds. Extrapolating from S+15's Fig 15, a threshold sufficient to give 0.05 false positives per 2×10^5 light curves, or 1 false positive per 4×10^6 light curves (as from our full frame images), is roughly 7.5. Making the same ad-hoc estimate that S+15 did and multiplying by 1.03 for the expected drop in SNR from cosmic ray noise gives a SNR threshold of 7.7 for full frame images. Considering our Fig. 15 (and noting the black line is for the sum of postage stamp and full frame image detections), adopting a SNR threshold of 7.7 for FFIs would mean a loss of $\sim 30 \times 4 = 120$ planets over two years, or 60 of what we claim are 'detected planets' from full frame images in 1 year's Extended Mission. We also note that our model lacks any accounting for time-correlated noise and the probabilistic nature of the signal recovery process, which are likely to be more important factors than the purely white-noise statistical fluctuations.
- 3.) We use synthetic stars from a single galactic model (TRILEGAL). One check on the robustness of this model would be to compare with other galactic models like GALAXIA [Sharma et al., 2011]

or the Besaçon model [Robin et al., 2003]. The simplest analytic model, applicable given that *TESS*'s limiting distance for $R_p < 4R_{\oplus}$ detections is $\lesssim 1$ kpc, is a distribution of stars uniform in the radial direction and with an exponential profile in the vertical direction. Independent of our numerical simulation, Winn [2013b] used such a galactic profile, with occurrence rates inferred from *Kepler* Q1-6. Our results are in order-of-magnitude agreement, with ours being slightly higher, likely due to our incorporation of Dressing and Charbonneau [2015]'s M dwarf occurrence rates.

It might eventually be best to use the real star catalog that *TESS*'s Target Selection Working Group is assembling. However, until *Gaia* DR2 (Q4 2017), this will likely come with large uncertainties on stellar radii, given the difficulty of distinguishing giants and sub-giants from M dwarfs without proper motions. An additional challenge is in companion fractions.

While we recommend that these broader checks be performed in future *TESS* yield calculations, they are excessive for the purposes of this report given that we only used the nearest, brightest, stars ($d \lesssim 1$ kpc, $I_c \lesssim 16$), with a simple prescription for background contamination, in evaluating *TESS*'s $R_p < 4R_{\oplus}$ detections. The uncertainties become much greater if we try to estimate detections of giant planets and false positives throughout the galactic disk. That said, we take S+15's cross-checks (cf Fig. 5 of that paper) against actual surveys of the local stellar population as indicative that we probably have the number of nearby stars, as well as their properties, correct for the accuracy required in this work.

- 4.) At least 2 transits for detection: recall Figs. 16 and 17. If we were to use a more stringent criteria, for instance at least 3 transits for detection as the *Kepler* pipeline currently does, we would lose $\mathcal{O}(200)$ of the planets detected in the Primary Mission, and $\mathcal{O}(100)$ from the Extended Missions. This assumption disproportionately affects long-period planets.
- 5.) We neglect instrument aging, spacecraft systematics, etc. To our knowledge detailed models do not currently exist for how *TESS*'s optics and CCDs will degrade with time. We are also assuming that, as with *K2*, time-correlated spacecraft level systematics can be removed in post-processing. These assumptions are reasonable at our current state of pre-flight knowledge, and will need to be changed accordingly as the mission progresses. If we were to assume a gradual decline in photometric performance, for instance from an increased number of dead or 'hot' pixels, the relative Extended-Mission-to-Extended-Mission comparisons would

remain identical. The absolute Extended-Mission-to-primary-Mission yields would decrease.

- 6.) We do not consider the efficacy of processing pipeline. For instance, `a11sky` will come with period ambiguities and aliasing problems imposed by its 14 day sampling at the ‘continuous’ viewing zones. Similar issues are generic across Extended Missions for which we detect a small number of transits in the Primary Mission, and then a small number of transits in the Extended Mission.

A robust way to approach this problem would be to generate a synthetic simulated *TESS* dataset, *i.e.*, at the image-level, rather than at the idealized phase-folded SNR level from this work, for each Extended Mission’s observations. Then actually perform astrometry on injected stars, extract light curves, de-trend them, and find their transits. This exercise would likely also be a useful way to prepare the SPOC and broader community for what we expect the era of *TESS* photometry to entail in terms of data quality.

4 Concluding remarks and recommendations

Although the science requirements for *TESS*’s Primary Mission have already been written [Ricker et al., 2014], an Extended Mission offers the entire astronomical community a chance to rethink and reprioritize the use of the spacecraft. A *TESS* Extended Mission would have wide-ranging applications, and should be planned and proposed with much broader goals than exoplanet science alone. The purpose of this trade study was to inform the exoplanet-related portion of that discussion. By simulating different scenarios for a third year of operations, we can anticipate the numbers and types of planets that would be discovered. Our study has also highlighted other issues, such as the ‘stale ephemerides’ problem, and the opportunity to change the selection of the PSs and the cadence of the FFIs for diverse reasons. This study was not designed to provide any definitive answers; but rather, to provide materials to use in further discussions. Our study has also prompted us to make some recommendations for future work that would be useful in this regard.

4.1 Recommendations

Deeper analysis of the target prioritization scheme. How should the results of the Primary Mission, or other sources of new data, be used to choose target stars for finer time sampling during an Extended Mission?

Optimize cadence. What is the optimal time sampling for transit detection? For example, observing 2×10^5 target stars at 4-minute cadence, rather than at 2-minute cadence, would allow the FFIs to be returned more frequently. This could in turn improve prospects for transit detection. (Preliminary numerical experiments indicate that this is indeed the case.)

In addition, a metric should be devised that quantifies, for each star, how much *improvement* would result from observing at a shorter cadence. Stars could then be prioritized according to this improvement statistic, rather than an overall planet-detectability statistic. For instance if the number of short-cadence stars could be greatly reduced with little effect on the planet detection statistics, then this might allow the FFIs to be returned at a higher cadence..

Take steps to address the ‘upgrading cadence’ problem: if there is a likely transiting planet in full frame image data, upgrading the planet to short cadence in future observing sectors improves the probability and fidelity of detection. How is this being addressed for the Primary Mission? Could this be an argument to observe the southern sky in year 3, in order to have extra time to prepare?

Solicit expert advice from experts in asteroseismology, transient detection, and other relevant areas to understand how the parameters of an Extended Mission would affect their scientific prospects. Comments on this report sent to the authors will be gratefully received. A more formal and comprehensive process would be a call for White Papers organized by the Guest Investigator program or the TESS Science Office. As exemplified in NASA’s 2016 Astrophysics Senior Review, everyone benefits from the discussions generated by such community feedback [Donahue et al., 2016].

Consider which of our proposed exoplanet metrics is most important. Sec. 1.3 summarizes these; the reader may have others to suggest. The crude metric of “total number of new planet detections” is not likely to be the most important, and we have found that the scenarios we considered differ by $\lesssim 30\%$ in this regard.

Simulate combining TESS and K2 data from ecl_long and ecl_short. This is perhaps the most important qualitative difference between observing towards and away from the ecliptic. Would TESS+K2 enable more discoveries out at long periods than alternatives? How many of the new planets that TESS detects on the ecliptic will actually be detected by K2? Is the value-added of combining datasets a compelling case compared with discovery?

Ensure pole adequately mitigates scattered sunlight. See description in Sec. 1.2.

Point of diminishing returns. Suppose, for example, the Primary Mission were repeated indefinitely. At what point would the planet discovery rate start falling significantly below that of Years 1-3? How much fainter would the host stars of new planets be, in each year?

Acknowledgements

We thank Peter Sullivan, for his support in the early phases of this work and for helpful comments on our results; Roland Vanderspek, for fielding numerous questions concerning *TESS* hardware; and Jack Lissauer, for input regarding the value of observing *Kepler*'s field with *TESS*. We thank the many other participants in informal discussions on this subject over the last few years. More broadly we are grateful to the hardworking teams at MIT, NASA Goddard, NASA Ames, CfA, STScI, Orbital Sciences, and other *TESS* partner institutions. We thank the *TESS* project for providing the computing resources used in this work, and Ed Morgan, Isaac Meister, and Kenton Philips for keeping those machines running.

Facilities: TESS, Kepler

Software: matplotlib [Hunter, 2007], NumPy [Walt et al., 2011], SciPy [Jones et al., 2001], pandas [McKinney], JPL NAIF's SPICE library [Acton, 1996], and the IDL Astronomy User's Library [Landsman, 1995].

Resources: This research has made use of the NASA Astrophysics Data System and the NASA Exoplanet Archive. The NASA Exoplanet Archive is operated by the California Institute of Technology, under contract with the National Aeronautics and Space Administration under the Exoplanet Exploration Program. This paper also makes use of data collected by the Kepler mission. Funding for the Kepler mission is provided by the NASA Science Mission directorate.

Appendices

A Models Relevant to Earth and Moon Crossings



Figure 25: Lens hood suppression plotted against the angular offset to a “point-source” like the Earth or Moon. This suppression factor is defined as the fraction of incident flux that is blocked by the spacecraft, sunshade, lens hood, or combinations thereof. Source: R. Vanderspek, priv. comm.

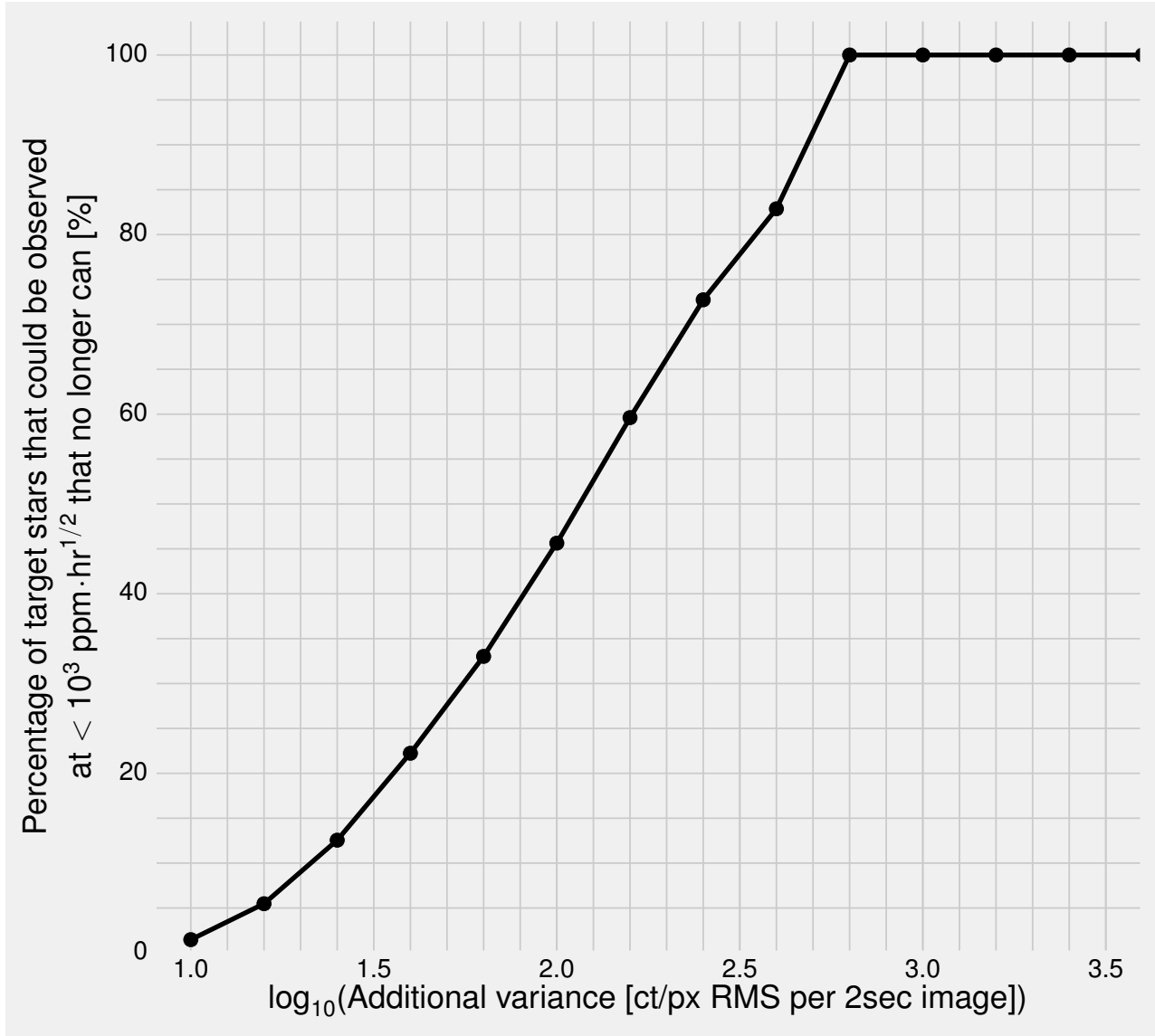


Figure 26: The procedure described in Sec. 1.6 flags fields to be dropped when there is a mean additional 300 ct/px/s from the Earth or Moon, corresponding to $\log_{10}(\text{Additional variance}) = 1.24$ on this plot. This reads that $< 10\%$ of the target stars which could be observed at $< 1\text{mmag}$ precision over 1 hour cannot when at F_{fresh} . While this corresponds to the cases with the Earth or Moon $\approx 28^\circ - 34^\circ$ from boresight, once closer, the effects become more serious. Saturation is assumed to occur at a mean flux $> 2 \times 10^5 \text{ ct/px per image}$. Lines between points intended to guide the eye.

B Lens Hood Model: Additional Count Rate from Arbitrary Source

Let $s(\theta)$ be the lens hood suppression as a function of angle θ from the camera boresight to a given point-source on the sky. By definition,

$$s(\theta) \equiv \frac{F_{\text{obs}}}{F_{\text{ns}}}, \quad (11)$$

for F_{obs} the observed flux of the source (that which reaches the CCD), and F_{ns} the flux that would be observed with no suppression and $\theta = 0$. The observed flux of the source can then be written as a function of θ

$$F_{\text{obs}}(\theta) = s(\theta)F_{\text{ns}} \quad (12)$$

$$= s(\theta)F_0 10^{-0.4(m_{\text{ns}} - m_0)}, \quad (13)$$

for F_0 the (non-suppressed) flux corresponding to a source with zero-point apparent magnitude m_0 , and m_{ns} the apparent magnitude of the source with no suppression. Winn [2013b] tabulates $F_0 = 1.6 \times 10^6 \text{ ph/s/cm}^2$ for an $I = 0$, G2V star. Thus

$$F_{\text{obs}}(\theta) = (1.6 \times 10^6)s(\theta)10^{-0.4m_{\text{ns}}} \quad [\text{ph/s/cm}^2]. \quad (14)$$

We can then write the following expression for $\mu \equiv F_{\text{obs}}A\eta/N$, the mean incident count rate on the pixel of interest:

$$\mu = (1.6 \times 10^6)s(\theta)10^{-0.4m_{\text{ns}}} \frac{A\eta}{N} \quad [\text{ct/px/s}], \quad (15)$$

for A the effective observing area in cm^2 , N the number of pixels per camera, and η the quantum efficiency. For TESS, $A = 69.1 \text{ cm}^2$, $N = 4096^2$, and $\eta \approx 1$. Using these numbers gives

$$\mu = 6.59s(\theta)10^{-0.4m_{\text{ns}}} \quad [\text{ct/px/s}]. \quad (16)$$

Assuming a Poisson arrival rate, the standard deviation in the number of counts per pixel per 2 second readout is then

$$\sigma \approx \mu^{1/2} = \left[13.2s(\theta)10^{-0.4m_{\text{ns}}} \right]^{1/2} \quad [\text{ct/px RMS per 2 sec image}]. \quad (17)$$

The above expression assumes that the scattered flux from the source is uniformly spread across the CCD. The reality may be quite different, but our purpose in this case is to simply get order-of-magnitude accuracy. Another caveat is that our zero-point relies on an I magnitude calibration – a more accurate approach would use separate bandpass-dependent zero-points.

To compute the net effect on TESS's noise budget, we add σ from Eq. 17 in quadrature with Eq. 2. We assume m_{ns} values of -26 , -13 , and -17.76 for the Sun, Moon, and Earth respectively. This gives Figs. 27-29.

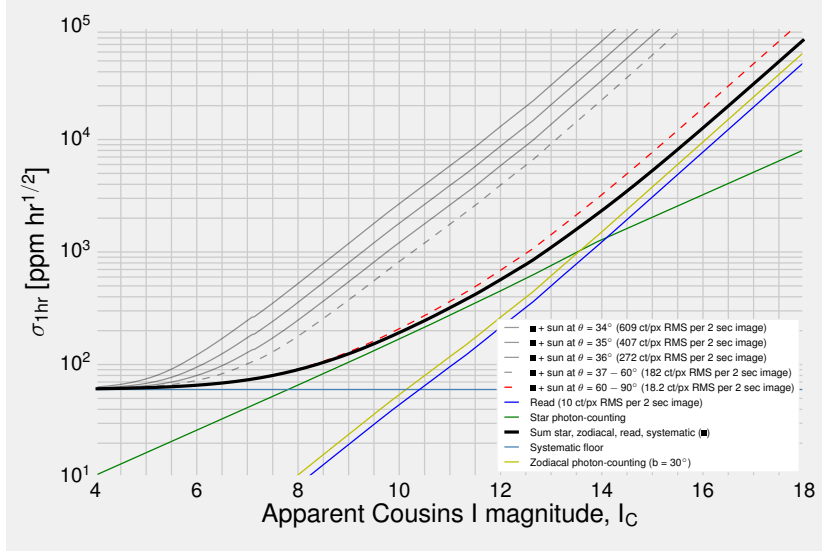


Figure 27: Noise budget including Solar scattered light at different angles θ from camera boresight. Note that the suppression model (Fig. 25) accounts solely for lens hood suppression, omitting sunshade suppression (which substantially lowers the dashed red line for most orientations of the Sun). The number given in brackets is σ in Eq. 17 – the extra standard deviation about the mean. Squaring, lines where $\mu \gtrsim 10^5$ ct/px/s will saturate the CCD pixels (and thus are not plotted).

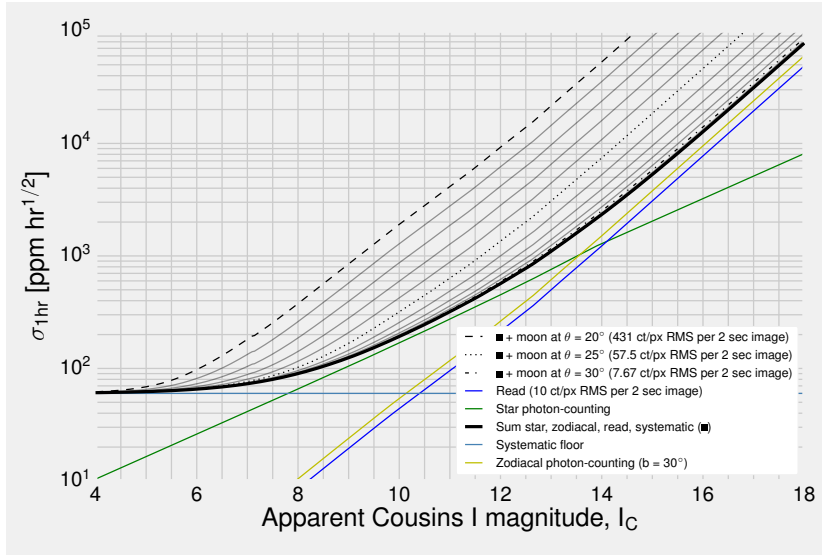


Figure 28: Same as Fig. 27, for scattered Moonlight. Gray lines are spaced by 1° .

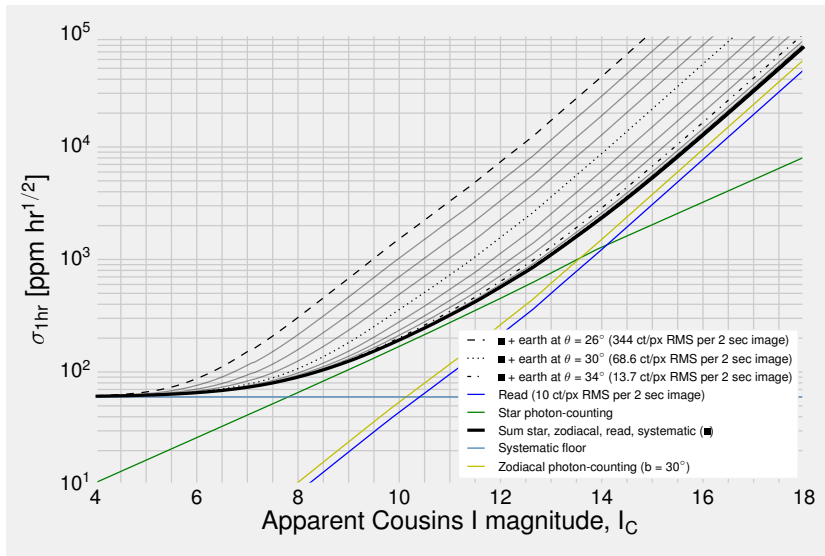


Figure 29: Same as Fig. 27, for scattered Earthlight. Gray lines are spaced by 1° .

C Changes from Sullivan et al. [2015]

Dilution bug. Described in Sec. 2.1.

Correction of coordinate assignment for multiple planet systems. In the code corresponding to S+15’s released catalog, “transiting objects” did not correctly inherit the coordinates of their parent star – they in fact received randomized coordinates within that star’s HealPix tile. While this is not a problem for the statistical results presented in S+15, it makes reverse-engineering multiple planet distributions from S+15’s Table 6 nearly impossible. The updated catalog associated with this white paper has coordinates which are unique system identifiers. An associated new column is a number (hostID), unique to each Monte Carlo realization of the updated code, with the same function.

On the angular dependence of TESS’s pixel response function: In our SNR calculation, we do not keep track of individual times for every transit. How then do we assign PSFs to different transits from the same object that fall on different regions of the CCDs, and thus should have slightly better or degraded PSFs? (Largest cumulative flux fraction at the CCD’s center, smallest at the corners).

S+15 dealt with this by computing the mean of all the field angles (distance from the center of the CCD axis), and then passing this mean into a look-up table for PSFs based on four PSFs that had been computed from a ray-tracing model at four different field angles. S+15 then ‘observes’ each eclipsing object with a single class of PSF. This leads to the implausible phenomenon that extra observations can actually *lower* the SNR of an eclipsing object if they are taken with an unfavorable field angle/PSF. This effect is largely off-set by the extra pointing increasing the SNR, but for Extended Missions (coming back to the same objects at potentially very different field angles) it winds up reducing observed SNR for $\sim 3\%$ of detected objects.

In Extended Missions (as well as in the Primary Mission) we expect stars to land on very different regions of the CCD over the course of being observed. We simplify this in our work by assuming that all stars land on the center of the *TESS* CCDs (the green curve of S+15 Fig. 13). This assumption is justified because our chief point of quantitative comparison is the ability of different pointing strategies to impact *TESS*’s planet yield in Extended Missions, and there is little *a priori* reason to assume that any one pointing scenario should be biased for an extra amount of stars to land on the ‘bad regions’ of *TESS*’s CCDs.

References

- C. H. Acton. Planetary data system: Ancillary data services of NASA's Navigation and Ancillary Information Facility. *Planetary and Space Science*, 44(1):65–70, Jan. 1996.
- I. Baraffe and G. Chabrier. Mass–Spectral Class Relationship for M Dwarfs. *ApJ*, 461(1), Apr. 1996.
- G. Basri, L. M. Walkowicz, and A. Reiners. Comparison of Kepler Photometric Variability with the Sun on Different Timescales. *ApJ*, 769(1):37, 2013.
- C. Beichman et al. Observations of Transiting Exoplanets with the James Webb Space Telescope (JWST). *PASP*, 126:1134–1173, Dec. 2014.
- C. J. Burke et al. Planetary Candidates Observed by Kepler IV: Planet Sample from Q1-Q8 (22 Months). *ApJ Supplement Series*, 210(2):19, 2014.
- C. J. Burke et al. Terrestrial Planet Occurrence Rates for the *Kepler* GK Dwarf Sample. *ApJ*, 809(1), Aug. 2015.
- J. A. Carter et al. Analytic approximations for transit light-curve observables, uncertainties, and covariances. *ApJ*, 689(1):499, 2008.
- D. Charbonneau et al. A super-Earth transiting a nearby low-mass star. *Nature*, 462(7275):891–894, Dec. 2009.
- D. Deming et al. Discovery and Characterization of Transiting Super Earths Using an All-Sky Transit Survey and Follow-up by the James Webb Space Telescope. *PASP*, 121(883):952, 2009.
- M. Donahue et al. 2016 NASA Astrophysics Senior Review. Technical report, NASA, Feb. 2016.
- C. D. Dressing and D. Charbonneau. The Occurrence of Potentially Habitable Planets Orbiting M Dwarfs Estimated from the Full Kepler Dataset and an Empirical Measurement of the Detection Sensitivity. *ApJ*, 807(1):45, 2015.
- D. A. Fischer and J. Valenti. The Planet-Metallicity Correlation. *ApJ*, 622:1102–1117, Apr. 2005.
- F. Fressin et al. The False Positive Rate of *Kepler* and the Occurrence of Planets. *ApJ*, 766(2):81, Apr. 2013.
- J. W. Gangestad et al. A high Earth, lunar resonant orbit for lower cost space science missions. *arXiv preprint arXiv:1306.5333*, June 2013.

- L. Girardi et al. Star counts in the Galaxy: Simulating from very deep to very shallow photometric surveys with the TRILEGAL code. *A & A*, 436(3):895–915, June 2005.
- G. M. H. J. Habets and J. R. W. Heintze. Empirical bolometric corrections for the main-sequence. *A & A Supplement Series*, 46:193–237, Nov. 1981.
- T. J. Henry et al. The solar neighborhood. XVII. Parallax results from the CTIOPI 0.9 m program: 20 new members of the RECONS 10 parsec sample. *AJ*, 132(6):2360, 2006.
- J. D. Hunter. Matplotlib: A 2d Graphics Environment. *Computing in Science & Engineering*, 9(3):90–95, 2007.
- J. A. Johnson et al. Giant Planet Occurrence in the Stellar Mass-Metallicity Plane. *PASP*, 122(894):905, 2010.
- E. Jones, T. Oliphant, P. Peterson, et al. Open source scientific tools for Python, 2001.
- C. H. Kepner and B. B. Tregoe. *Rational Manager*. 1965.
- D. M. Kipping and C. Lam. Transit Clairvoyance: Enhancing TESS follow-up using artificial neural networks. June 2016.
- R. K. Kopparapu et al. Habitable Zones Around Main-Sequence Stars: New Estimates. *ApJ*, 765(2):131, Mar. 2013.
- W. B. Landsman. The IDL Astronomy User’s Library. volume 77, page 437, 1995.
- L. Lyons. *A Practical Guide to Data Analysis for Physical Science Students*. Cambridge University Press, Nov. 1991. ISBN 978-0-521-42463-9.
- T. Mazeh, T. Holczer, and S. Faigler. Dearth of short-period Neptunian exoplanets - a desert in period-mass and period-radius planes. *A & A*, 589:A75, May 2016.
- W. McKinney. pandas: a foundational python library for data analysis and statistics.
- S. M. Mills et al. A resonant chain of four transiting, sub-Neptune planets. *Nature*, 533(7604):509–512, May 2016.
- M. A. C. Perryman et al. The HIPPARCOS Catalogue. *A & A*, 323, July 1997.

- E. M. Price and L. A. Rogers. Transit Light Curves with Finite Integration Time: Fisher Information Analysis. *ApJ*, 794(1):92, Sept. 2014.
- G. R. Ricker et al. Transiting Exoplanet Survey Satellite. *Journal of Astronomical Telescopes, Instruments, and Systems*, 1(1), Oct. 2014.
- A. C. Robin, C. Reylé, S. Derrière, and S. Picaud. A synthetic view on structure and evolution of the milky way. *A & A*, 409(2):523–540, 2003.
- S. Sharma, J. Bland-Hawthorn, K. V. Johnston, and J. Binney. Galaxia: a code to generate a synthetic survey of the Milky Way. *ApJ*, 730(1):3, Mar. 2011.
- P. W. Sullivan et al. The Transiting Exoplanet Survey Satellite: Simulations of Planet Detections and Astrophysical False Positives. *ApJ*, 809(1):77, Aug. 2015.
- F. van Leeuwen. Validation of the new Hipparcos reduction. *A & A*, 474(2):12, 2007.
- S. v. d. Walt, S. C. Colbert, and G. Varoquaux. The NumPy Array: A Structure for Efficient Numerical Computation. *Computing in Science & Engineering*, 13(2):22–30, Mar. 2011.
- J. Wang and D. A. Fischer. Revealing a Universal Planet–Metallicity Correlation for Planets of Different Sizes Around Solar-type Stars. *AJ*, 149(1):14, 2015.
- J. N. Winn. Expected photon fluxes in the TESS bandpass. *TESS Science Memo No. 1, Version 2. Available upon request.*, 2013a.
- J. N. Winn. Number of Searchable Stars. *TESS Science Memo No. 5, Version 1. Available upon request.*, 2013b.